Neutron scattering studies of hydrogenated, deuterated and fluorinated amorphous silicon

2007 J. Phys.: Condens. Matter 19 415109

(http://iopscience.iop.org/0953-8984/19/41/415109)

IOP PUBLISHING JOURNAL OF PHYSICS: CONDENSED MATTER

J. Phys.: Condens. Matter **19** (2007) 415109 (33pp) doi:10.1088/0953-8984/19/41/415109

Neutron scattering studies of hydrogenated, deuterated and fluorinated amorphous silicon*

Adrian C Wright[1], Alex C Hannon[2], Roger N Sinclair[1], Thierry M Brunier[1], Carlo A Guy[1], Roger J Stewart[1], Matthias B Strobel[1] and Frank Jansen[3]

[1] J J Thomson Physical Laboratory, University of Reading, Whiteknights, Reading RG6 6AF, UK
[2] ISIS Facility, Rutherford Appleton Laboratory, Chilton, Didcot, Oxon OX11 0QX, UK
[3] Xerox Corporation, Joseph C Wilson Center for Technology, Rochester, NY 14644, USA

E-mail: a.c.wright@rdg.ac.uk

Received 1 June 2007, in final form 14 August 2007
Published 27 September 2007
Online at stacks.iop.org/JPhysCM/19/415109

Abstract

A comprehensive neutron scattering study has been performed of hydrogenated ($Si_{0.78}H_{0.22}$), deuterated ($Si_{0.77}D_{0.23}$) and partially fluorinated deuterated ($Si_{0.725}D_{0.120}F_{0.155}$) amorphous silicon, prepared by the glow-discharge technique. The measurements performed include diffraction, small-angle neutron scattering (SANS) and inelastic neutron scattering, and the data obtained are discussed in terms of various structural models in the literature. The real-space correlation function for $Si_{0.77}D_{0.23}$ exhibits sharp peaks at 1.49 and 2.36 Å, due to Si–D and Si–Si covalent bonds, respectively, while peaks centred at 3.2 and 3.8 Å are due to Si–D and Si–Si second-neighbour distances. High-energy resolution inelastic scattering measurements for $Si_{0.78}H_{0.22}$ show that there are approximately equal numbers of $\equiv$SiH and $=SiH_2$ groupings, there being no indication of excitations corresponding to $-SiH_3$ groupings. The presence of molecular hydrogen is demonstrated unambiguously by the observation of the ortho-to-para conversion, via molecular rotation modes at 14.5 and 29.4 meV. The shift in the Si–H stretch modes introduced by deuteration is slightly less than the value of $\sqrt{2}$ expected for free hydrogen, indicating a small but observable influence of the amorphous silicon matrix. The size of the cages containing the H_2 molecules has been investigated via SANS, which yields a mean Guinier radius of ~5–6 Å. In addition, the use of the H–D SANS contrast technique indicates that each cage contains on average about 60 H_2 (D_2) molecules. The data for the $Si_{0.725}D_{0.120}F_{0.155}$ sample are consistent with a previously suggested model of network cages predominantly containing molecular SiF_4.

(Some figures in this article are in colour only in the electronic version)

* Paper submitted for inclusion in the Festschrift in honour of Spencer Howells.

1. Introduction

Hydrogenated amorphous silicon is a most important but complicated technological material. Despite its widespread use, for example in xerography, solar cells and flat-panel liquid crystal displays [1, 2], its structure and properties are poorly understood, particularly in respect of the role played by the hydrogen atoms. In particular, understanding the way in which hydrogen affects the electronic properties and hence the electronic density of states requires accurate data on both the atomic structure and dynamics. A comprehensive neutron scattering investigation has therefore been performed of hydrogenated ($Si_{0.78}H_{0.22}$), deuterated ($Si_{0.77}D_{0.23}$) and partially fluorinated deuterated ($Si_{0.725}D_{0.120}F_{0.155}$) glow-discharge amorphous silicon, involving diffraction, inelastic scattering and small-angle neutron scattering (SANS), using instruments at the ISIS spallation pulsed neutron source and at the high-flux reactor at the Institut Laue-Langevin (Grenoble, France). A survey of the instruments at ISIS, suitable for studying amorphous silicon materials, has been published by Howells [3], and several of these instruments have been employed in this work. The present paper will report hitherto unpublished diffraction data on all three samples, summarize the important results from the earlier inelastic scattering [4–6] and SANS measurements [7], together with further analysis and new inelastic scattering data, and provide a unified interpretation of the combined data set, thus acting as a final report on these studies. A comparison will also be made with the various structural models proposed in the literature and outlined below.

Detailed reviews of previous studies of the structure and dynamics of hydrogenated amorphous silicon have been given by Knights [8] and by Elliott [9], and so only a brief summary of the most important results will be presented here. Initially, it was thought that the material prepared by the glow-discharge decomposition of silane (SiH_4) did not contain hydrogen but comprised a continuous random network, along the lines of that suggested for evaporated Si and Ge and represented in an idealized, defect-free form by the structural models of Polk and Boudreaux [10], Wooten and Weaire [11], etc. (See [12] and [13] for a discussion of these models and a comparison with neutron data for amorphous Ge.) This idealized structure is illustrated schematically in two dimensions, using three-connected Si atoms, in figure 1(A). However, in reality, the latter materials contain significant numbers of broken bonds, as detected by electron spin resonance (ESR) spectroscopy ($\sim 10^{19}$–10^{20} spins cm^{-3} [14, 15]), which lead to states in the gap that contribute to the optical absorption and electronic conduction processes. These states act as non-radiative recombination centres with the result that photoconductivity and photoluminescence are small, and hence pure amorphous Si is of very limited use as an electronic material. It was thus realized that, in the glow-discharge material, these broken bonds are passivated by hydrogen atoms to form Si–H bonds, as shown on the left-hand side of figure 1(B).

Several diffraction and extended x-ray absorption fine structure (EXAFS) studies of glow-discharge hydrogenated amorphous silicon have been reported in the literature [16–26], and they are summarized in table 1. Neutron diffraction is a more powerful technique than x-ray or electron diffraction, when studying glow-discharge hydrogenated amorphous silicon, since hydrogen has only one electron and hence does not contribute appreciably to the overall x-ray or electron scattering. As a result, x-ray [16, 17] and electron [18, 19] diffraction measurements are dominated by the scattering from Si and yield very little information on the structural role of the H atoms. The x-ray data of Shülke [17], for glow-discharge material of composition $Si_{0.67}H_{0.33}$, yield a mean Si–Si bond length of 2.363 ± 0.008 Å and a second Si–Si coordination shell at 3.86 Å. The Si–$\hat{\text{Si}}$–Si bond angle, β_{Si}, variation is $7.9° \pm 0.4°$, and the first-neighbour Si–Si coordination number, $n_{\text{Si(Si)}}$, is 3.4 ± 0.1. The structure above 3 Å in the real-space correlation function was interpreted as being due to a mixture of 35% staggered (bond torsion

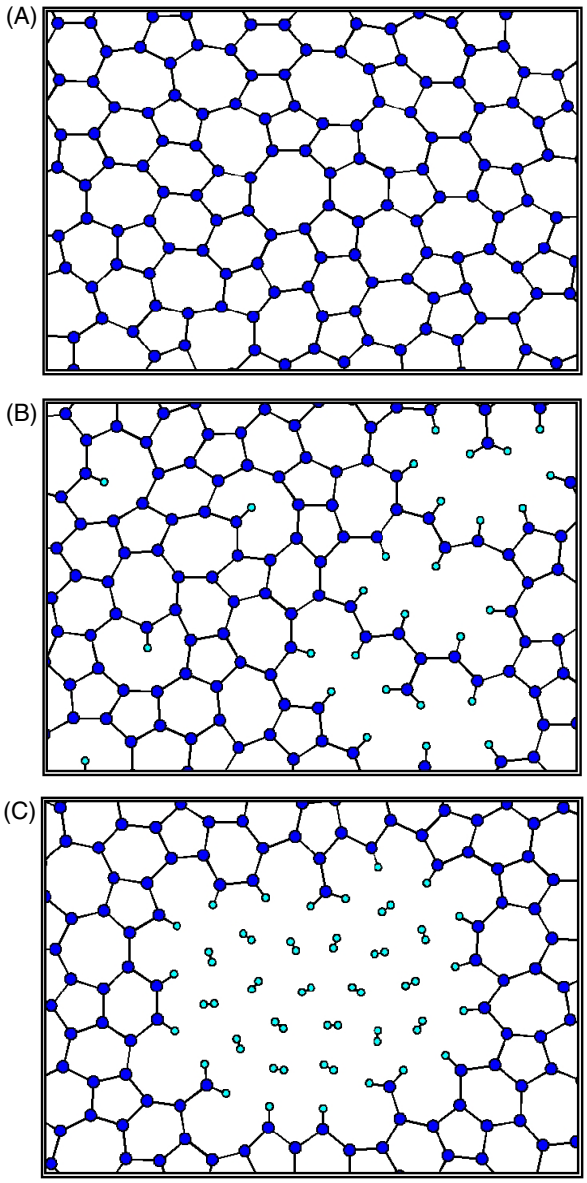

Figure 1. Two-dimensional (2D) schematic diagrams showing (A), a continuous amorphous Si network; (B), hydrogenated amorphous silicon with terminal Si–H bonds and a disordered boundary region; and (C), a Si network cage containing H_2 molecules. The larger blue (or darker) atoms are Si and the smaller cyan (or lighter) atoms H. In reality, the van der Waals radius for hydrogen is much larger than the radius employed in (B) and (C), and the H_2 molecules in (C) are in a highly compressed state. Hence they are very much closer to each other, and to the terminal H atoms lining the cage walls, than might be inferred from this diagram.

(dihedral) angle, $\alpha = 0°$), 45% eclipsed ($\alpha = 60°$) and 20% 'middle' ($\alpha = 35°$–$45°$) configurations of adjacent tetrahedra. In general, x-ray and electron diffraction studies suggest that the Si network of the hydrogenated material is similar to that for evaporated amorphous silicon, but with the broken bonds saturated with H atoms.

Table 1. Diffraction and EXAFS studies.

Ref.	Author(s)	x[a]	Method	$r_{\mathrm{Si-H}}$ (Å)	$n_{\mathrm{Si(Si)}}$	$r_{\mathrm{Si-Si}}$ (Å)	$r_{\mathrm{Si-(2)Si}}$ (Å)
[16]	Mosseri *et al*	0.33	X-ray	—	3.5	2.38	—
[17]	Schülke	0.33 ± 0.02	X-ray	—	3.40 ± 0.10	2.363 ± 0.008	3.86 ± 0.01
[18]	Barna *et al*	—	Electron	—	4.0 ± 0.5	2.35	—
[19]	Graczyk	0.20–0.40	Electron	—	$3.55–3.25 \pm 0.1$	2.375 ± 0.05	3.69 ± 0.05
[20]	Postol *et al*	∼0.14	Neutron	—	—	—	—
[21–24]	Bellissent *et al*	0.16	Neutron	1.48	—	2.35	3.84
[25]	Filipponi *et al*	0.14	EXAFS	—	3.92 ± 0.16	2.35 ± 0.01	—
		0.21	EXAFS	—	3.60 ± 0.16	2.36 ± 0.02	—
[23, 26, 27]	Menelle *et al*		EXAFS	—	3.78		—

[a] Composition: $Si_{1-x}H_x$.

An additional advantage with neutron diffraction is that the H–D isotopic substitution technique can be used to (partially) separate the individual component real-space correlation functions [20–24]. On the other hand, the analysis of neutron data for samples containing hydrogen is hampered by the large incoherent scattering cross section for ^{1}H, and so very high statistical accuracy is required when recording the diffraction pattern. The low atomic mass of H and D also make it difficult to make (Placzek) corrections for departures from the static approximation. Neutron diffraction experiments have been performed [20] on sputtered amorphous Si, Si–H and Si–D with approximately 14% H/D concentrations. The data were not taken to sufficiently high scattering vector magnitudes, Q, ($Q_{\mathrm{max}} = 8.75$ Å^{-1}) to obtain good real-space resolution, although it was concluded that the structure of amorphous Si was not significantly altered by the inclusion of large amounts of hydrogen. The isotopic substitution technique has also been employed by Bellissent and co-workers [21–24] ($Q_{\mathrm{max}} = 16$ Å^{-1}) to separate the Si–Si, Si–H and H–H component correlation functions for sputtered hydrogenated amorphous silicon containing 16 at.% hydrogen. Three samples were used, of composition $Si_{0.84}H_{0.16}$, $Si_{0.84}H_{0.10}D_{0.06}$ and $Si_{0.84}D_{0.16}$.

Filipponi *et al* [25] have investigated glow-discharge hydrogenated amorphous silicon using EXAFS spectroscopy and compared this material with crystalline and sputtered amorphous silicon. A similar comparison of EXAFS measurements on sputtered hydrogenated amorphous silicon, crystalline and amorphous silicon [23, 26, 27] indicates small changes in the shape of the first (Si–Si) peak in the pair-correlation function, but the total coordination number for Si is unchanged. It is concluded that the structure of amorphous silicon is heterogeneous, rather than homogeneous, and that hydrogenated amorphous silicon should be regarded as being similar to pure amorphous silicon but with the broken bonds decorated with hydrogen and having a heterogeneous distribution of hydrogen; i.e. with hydrogen-rich regions.

Small-angle x-ray scattering (SAXS) [28–30], SANS [20, 22, 31–37] experiments and electron microscopy [18, 35, 38] all indicate that glow-discharge hydrogenated amorphous silicon is normally heterogeneous and consists of sections of a more-or-less continuous network linked by highly disordered (boundary) regions (figure 1(B)—note that, in the real material, the disordered boundary regions are much thicker than shown in this schematic diagram). More specifically, depending on the preparation conditions, a columnar microstructure may be observed [18, 38], which is characteristic of thin-film preparation techniques. Leadbetter *et al* [29, 31] find that anode-deposited glow-discharge samples have a columnar morphology with a dominant column diameter of ∼60 Å. From their SANS measurements on sputtered samples, Postol *et al* [20] and Bellissent *et al* [32–34, 36, 37] obtain radii of gyration of ∼270 and ∼125 Å, respectively. Bellissent and co-workers [32, 34, 35] also observe a diffraction ring

at 0.22 $Å^{-1}$, suggesting a possible correlation length of ∼30 Å. The intensity of the SANS decreases with the hydrogen isotope concentration, from which it is inferred that hydrogen clusters are present in the matrix [32–34]. Antonio and Konnert [28] have performed SAXS measurements on glow-discharge hydrogenated amorphous silicon and conclude that the void distribution for this material is very similar to that for evaporated amorphous silicon.

As discussed in [2], it has been suggested, as a result of nuclear magnetic resonance (NMR) [15, 39–47] and infra-red (IR) [48, 49] measurements, that a significant fraction of the hydrogen is present in the form of H_2 molecules trapped under high pressure within the cages defined by the amorphous covalent network (figure 1(C)) and that this molecular hydrogen undergoes a very broad solid–fluid transition between ∼20 and ∼30 K, a temperature considerably higher than the melting and boiling points for normal (*n*-) H_2 at atmospheric pressure (13.8 and 20.3 K, respectively [50]). (Note that, at normal pressure, the H–H stretching mode for molecular H_2 is not IR active.) This temperature indicates that the H_2 is under considerable pressure (∼2 kbar [48]). In addition, the NMR studies show that orientational ordering may take place at ∼20 K [41]. More recent studies [46] report the gradual ortho–para conversion of the trapped D_2 in the deuterium analogue at 4.2 K and outline the effects of annealing and deposition rate on these properties [45]. In addition to the high-pressure H_2 found in hydrogenated amorphous silicon, molecular SiF_4 is also known to exist in the fluorine-doped derivatives [51–54]. For samples prepared by photochemical vapour deposition, Langford *et al* [54] have suggested that these SiF_4 molecules are contained within cages of much the same size as those containing the molecular H_2 in the hydrogenated material.

Structural models of the network component of hydrogenated amorphous silicon have been published by Weaire *et al* [55, 56], Guttman [57] and Winer and Wooten [58]. The Weaire *et al* model is in the form of an approximately spherical cluster, comprising a total of 397 atoms (314 Si and 83 H), while that of Winer and Wooten has been generated with a periodic boundary. The latter model has 105 atoms (81 Si and 24 H), and Winer and Wooten [58] have also calculated the full vibrational spectrum for their model, together with the density of vibrational states involving only the motion of the hydrogen atoms. Of the 24 H atoms, two are involved in a single $=SiH_2$ group, while the other 22 are in ≡SiH groups. A different approach, comprising a heterogeneous system with local defects, has been employed by Sadoc and Mosseri [59] and by Rivier and Duffy [60].

The growth of thin films of hydrogenated amorphous silicon is principally controlled by the phenomena of absorption, desorption, surface mobility and nucleation, all of which are strongly influenced by the preparation method/conditions. Thus, given the variability of preparation techniques and conditions, it is vital to obtain dynamical and structural data on the same, well-characterized sample(s). Previous neutron scattering studies of hydrogenated amorphous silicon and related materials have been hampered by the small quantities of sample available, and so much larger samples of hydrogenated ($Si_{0.78}H_{0.22}$), deuterated ($Si_{0.77}D_{0.23}$) and partially fluorinated deuterated ($Si_{0.725}D_{0.120}F_{0.155}$) amorphous silicon have been prepared for the present studies by the glow-discharge technique.

High-resolution measurements of the inelastic scattering are required to investigate the vibrational modes of the system to check the interpretation of IR and Raman spectra [61, 62] and to look for modes which may be missed in the optical spectra because of selection rules. Neutron measurements are useful because they are free from the problem of selection rules and the spectral dependence of the coupling of the electromagnetic radiation to the vibrational excitations. Inelastic neutron scattering also offers added possibilities for mode assignment through the Q dependence of a chosen mode, as revealed in the dynamic structure factor, $S(Q, E)$. This, combined with the freedom from matrix element effects which can confuse the interpretation of optical spectroscopic results, should give unambiguous information with

regard to the short-range structure in network amorphous solids. The experimental difficulty is to provide energy transfer resolution which can match that offered by Raman and IR techniques. With each increase in neutron source intensity, advances in this direction can be made, and examples of this are given in the following sections. In particular, the results obtained with the instrument MARI [63] at the ISIS pulsed neutron source (Rutherford Appleton Laboratory, UK) show that new information is obtained with each increase in resolution.

Although the existence of trapped high-pressure molecular H_2 is now well documented [5, 6, 9, 39–49], very little is known about its local environment. That the H_2 is confined within network cages would seem a necessity of its nature, but the size, shape, number, and distribution of these regions is still uncertain. In the present study, SANS has been employed to investigate the regions containing H_2 (D_2) in amorphous $Si_{0.78}H_{0.22}$($Si_{0.77}D_{0.23}$). SANS is better suited to this task than is small-angle x-ray scattering (SAXS), since the hydrogen contrast is small for x-rays and, for neutrons, H–D isotopic substitution can be used to separate the fluctuations in the H/D density from those of the amorphous silicon matrix. A SANS investigation has also been carried out on amorphous $Si_{0.725}D_{0.120}F_{0.155}$, to examine the local environment of the SiF_4 molecules.

2. Experimental procedures

2.1. Sample preparation

The samples used in these studies were prepared at the Xerox Webster Research Center (USA) by the glow-discharge decomposition of electronic-grade source gases in a cylindrical cross-flow reaction chamber (xerographic drum coating unit) [64]. The inner rotating drum (diameter 240 mm and length 400 mm) was covered with an iron-free aluminium sheet (thickness 50 μm) which served as a cathode in the deposition process. The inner diameter of the electrically grounded counter-electrode was 280 mm. The deposition system was checked for leak tightness before each run, typical leakage rates being approximately six orders of magnitude lower than the gas flow rate.

A DC discharge was created in the annular space between the electrodes by applying a negative potential (1250 V) to the heated inner electrode (substrate, 230 °C). The total current was sustained at a constant 300 mA during the deposition. Prior to each run, the apparatus was cleaned by removing all previous deposits and cleaning in an Ar/H_2 (or Ar/D_2) atmosphere. The deposition of the hydrogenated and deuterated amorphous silicon films was carried out at a pressure of 250 mTorr of SiH_4 or SiD_4 (98% D, Cambridge Isotope Laboratories, Inc.), respectively. The gas flow rate into the chamber was 200 cm^3 min^{-1} and two films were deposited in runs of typically 4.5 h each. The fluorinated amorphous silicon film was deposited at 250 °C, by flowing a mixture of SiF_4 (140 cm^3 min^{-1}) and D_2 (25 cm^3 min^{-1}) at a pressure of 700 mTorr. Again, a DC discharge was maintained (−500 V, 500 mA), this time for 14 h, at which time the SiF_4 feedstock ran out.

The aluminium substrates were removed from the deposited films by dissolving in 10% HCl (DCl), after which the films were thoroughly washed in H_2O (D_2O) to remove any traces of $AlCl_3$. The film flakes were then vacuum dried at 70 °C. The dissolution of the Al substrate was performed in a dry-box under a continuous purge of dry nitrogen.

Table 2 summarizes some of the physical properties of the present samples. The compositions were determined by NMR analysis, which indicates that, within the precision of ±2 at.%, the hydrogenated and deuterated samples contain the same amount of H/D. The NMR data also indicate that the amorphous $Si_{0.77}D_{0.23}$ contains 3% D_2 and 1% –SiD_3 groups. Band gaps were determined by measuring the optical absorption as a function of

Table 2. Sample parameters.

	$Si_{78}H_{22}$	$Si_{77}D_{23}$	$Si_{72.5}F_{15.5}D_{12}$
NMR analysis			
At.% H	22 ± 2[a]	—	—
At.% D	—	23 ± 2[b]	12
At.% F	—	—	15.5
IR analysis			
At.% H	21	—	—
At.% D	—	24	—
Metallic impurities (ppm)	<2	<2	<2
Band gap (eV)	1.72	1.75	—
ESR density (spins cm^{-3}, $g = 2.0054$)	1.1×10^{16}	9.8×10^{15}	1.7×10^{16}
Xerographic charging (V μm^{-1}) (−)	2 + PD[c]	2 + PD[c]	—
Xerographic charging (V μm^{-1}) (+)	2	2	—
$\Sigma_i \bar{b}_i$ (10^{-14} m)	0.241 37	0.472 91	0.468 50

[a] Includes unbonded H_2.
[b] Includes 3 at.% D as D_2 and 1 at.% D in $–SiD_3$ groups.
[c] Photodischarge.

wavelength and extrapolating the results on a Tauc plot [65]. The xerographic data show that the $Si_{0.77}D_{0.23}$ sample is slightly n-type and has an electron range exceeding 25 μm. This is typical behaviour for undoped hydrogenated amorphous silicon. The spin densities measured by ESR are typical of cathodically deposited DC materials and quite acceptable for xerographic applications, although somewhat higher than for anodically deposited material. The $Si_{0.78}H_{0.22}$ and $Si_{0.77}D_{0.23}$ samples are analytically pure, show typical optical and electronic characteristics and are nominally the same. No optical or electrical measurements were performed on the fluorinated material due to its poor adhesion to glass substrates.

To extract the real-space total correlation function, $T(r)$, from the diffraction data, it is necessary to know the average number density, ρ^0, and the total scattering amplitude per composition unit (c.u.). For the present samples, the data are normalized to a composition unit containing a total of one atom. A complication with materials containing voids is that the mass density used to calculate ρ^0 should be that of the bulk material, excluding the void volume. Hence a measurement of the mass density yields a lower limit for ρ^0.

The mass density of the $Si_{0.78}H_{0.22}$ sample was determined to be 2.063 ± 0.003 g cm^{-3}, using a Quantachrome micropycnometer with helium as the measurement gas. This is similar to the values obtained by other authors; namely 2.02 g cm^{-3} for $Si_{0.67}H_{0.33}$ [17] and 2 g cm^{-3} for $Si_{0.65}H_{0.35}$ [16]. Helium was used since it is the most penetrating of the rare gases. The mass density yields an average number density of $\rho^0 = 0.056\,14 \pm 0.000\,08$ c.u. $Å^{-3}$, corresponding to a silicon atom number density of $\rho^0_{Si} = 0.043\,79 \pm 0.000\,06$ atoms $Å^{-3}$, which is ∼88% of that for crystalline Si ($\rho^0_{Xtal} = 0.04\,994$ atoms $Å^{-3}$ [66]). Similarly, Graczyk [19] quotes a silicon atom density of ∼79% of the crystalline value for both glow-discharge $Si_{0.80}H_{0.20}$ and $Si_{0.75}H_{0.25}$. In the analysis of the diffraction data, to allow use of the H–D isotopic substitution technique, it was assumed that the H/D content of the hydrogenated and deuterated samples is the same; i.e. that $x_H = x_D = 0.225$. The resulting values for the total scattering amplitude per c.u. are given in table 2, the neutron scattering lengths, $\bar{b}_{Si} = 0.414\,91 \times 10^{-14}$ m, $\bar{b}_H = -0.373\,90 \times 10^{-14}$ m, $\bar{b}_D = 0.6671 \times 10^{-14}$ m and $\bar{b}_F = 0.5654 \times 10^{-14}$ m being taken from Sears [67].

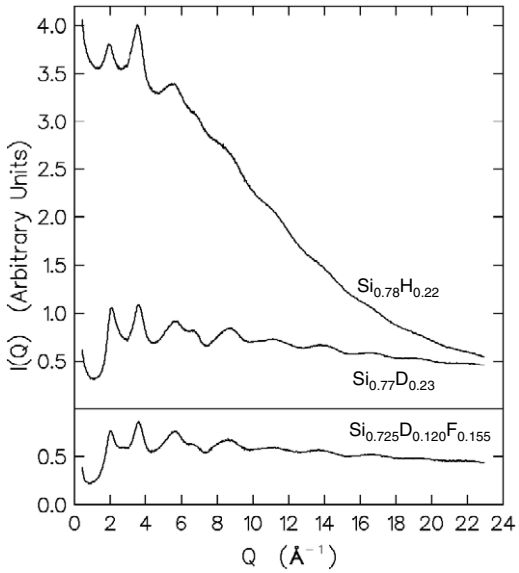

Figure 2. Background-corrected diffraction patterns for the three samples obtained with the ILL D4b diffractometer. The turn up at low Q is small-angle scattering.

2.2. Neutron diffraction

A discussion of the neutron diffraction technique and a summary of the formalism employed here can be found in [68]. Neutron diffraction patterns were recorded for all three samples, using the D4b diffractometer at the Institut Laue-Langevin (ILL), and are shown in figure 2. The maximum scattering vector magnitude, $Q_{\max}$, is 22.95 Å^{-1}. A cubic spline fit was made to each diffraction pattern, following subtraction of the empty sample can background. The diffraction patterns were corrected for absorption and multiple scattering [69]. However, the presence of either H or D atoms in the samples meant that it was not possible to use the analytical form for the Placzek corrections for departures from the static approximation [69], and so the self-scattering, $I^{\mathrm{S}}(Q)$, was obtained by an iterative procedure based on a polynomial fit to the highly smoothed intensity data, generated via a running 101 point average. The final self-scattering for $Si_{0.77}D_{0.23}$ is shown in figure 3, together with the corrected, normalized diffraction pattern, $I(Q)$. The data for $Si_{0.78}H_{0.22}$ and $Si_{0.77}D_{0.23}$ have been extended to higher scattering vector magnitudes ($Q_{\max} = 28.485$ Å^{-1}), by combining them with data obtained from the ISIS LAD spectrometer 150° detector bank. Similar corrections were performed for these data, and again it was necessary generate $I^{\mathrm{S}}(Q)$ iteratively, using the same procedure. The reasons for the relatively low $Q_{\max}$, despite the fact that the LAD instrument is capable of recording data up to 60 Å^{-1}, is that the samples do not scatter strongly and the Si tetrahedra in the amorphous network are distorted, leading to oscillations in the interference function, $Qi(Q)$, which decay rapidly at high Q. The final interference function, $Qi(Q)$, for $Si_{0.77}D_{0.23}$ is shown in figure 3 and the real-space total correlation functions, $T(r)$, for all three samples in figure 4. To allow a direct comparison, all three correlation functions in figure 4 were generated with the same value of $Q_{\max}$ (22.95 Å^{-1}). The higher-resolution real-space correlation functions for the deuterated and hydrogenated samples, obtained from the combined D4b and LAD data, are shown later in section 3 (figure 12). Due to the problems in calculating the self-scattering, the vanadium-

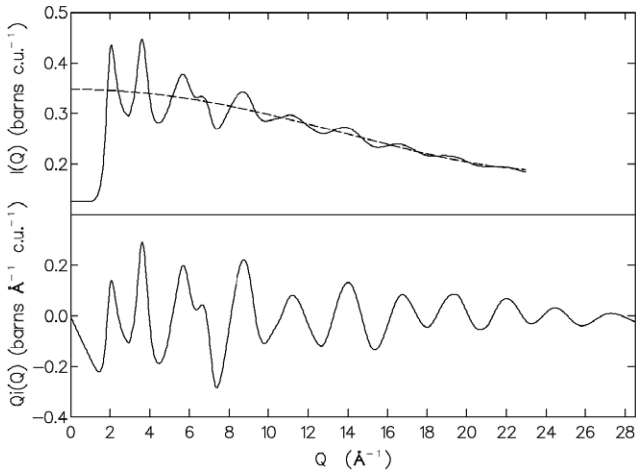

Figure 3. Upper curves: the corrected, normalized diffraction pattern, $I(Q)$ (solid line—cubic spline fit with the SANS contribution removed) for $Si_{0.77}D_{0.23}$, from D4b, together with the self-scattering (dashed line). Lower curve: the combined (D4b + LAD) interference function, $Qi(Q)$.

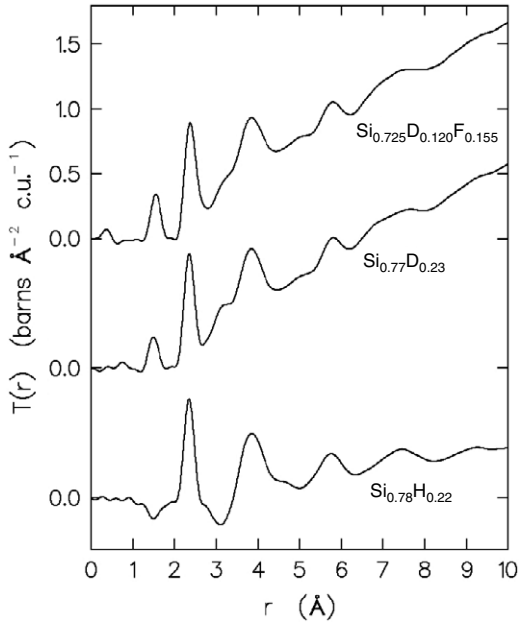

Figure 4. The real-space total correlation functions, $T(r)$, for the three samples (Q_{max} = 22.95 Å^{-1}).

normalized diffraction patterns were renormalized to be consistent with the measured average density for the $Si_{0.78}H_{0.22}$ sample. In the case of $Si_{0.725}D_{0.120}F_{0.155}$, it is assumed that the Si network density is the same as that for $Si_{0.78}H_{0.22}$.

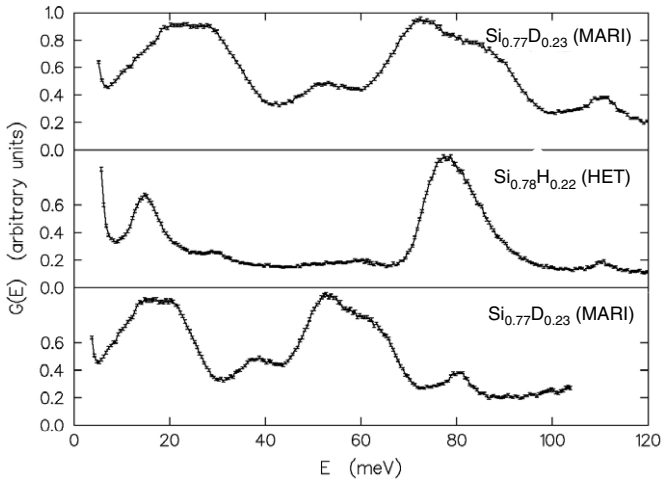

Figure 5. The inelastic neutron scattering from $Si_{0.78}H_{0.22}$ and $Si_{0.77}D_{0.23}$ measured using the ISIS HET and MARI spectrometers with $E_0 = 129.9$ meV (HET) and $E_0 = 108.7$ meV (MARI). The sample temperature is 20 K. For the top curve, the energy scale for the deuterated sample has been multiplied by 1.373 (see the text).

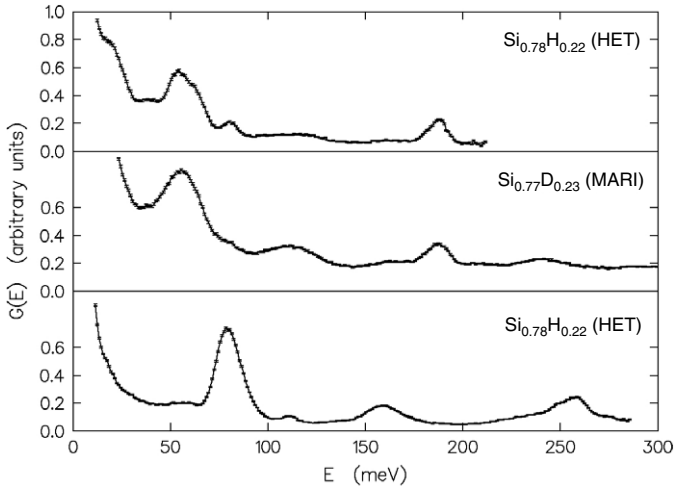

Figure 6. The inelastic neutron scattering at 20 K for $Si_{0.78}H_{0.22}$, from the ISIS HET spectrometer ($E_0 = 292.8$ meV), and that for $Si_{0.77}D_{0.23}$ obtained with both the HET ($E_0 = 220$ meV) and MARI spectrometers ($E_0 = 398.3$ meV).

2.3. Inelastic neutron scattering

Measurements of the neutron-weighted vibrational density of states have been performed using both the HET and MARI spectrometers at the ISIS pulsed neutron source and a range of incident neutron energies, E_0, to allow the optimum energy transfer resolution to be obtained for selected regions of the spectra [6]. Figure 5 compares the uncorrected scattering functions, $S(Q, E)$, for the hydrogenated and deuterated samples, while figure 6 provides a similar comparison at higher E_0 values, to allow inclusion of the Si–H/D stretching modes.

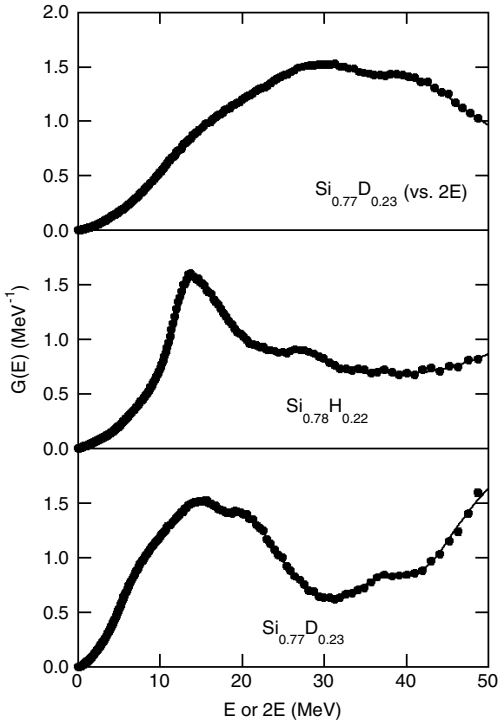

Figure 7. The effective vibrational density of states for $Si_{0.78}H_{0.22}$ and $Si_{0.77}D_{0.23}$ at 100 K, as measured with the IN6 spectrometer at the ILL. In the top curve, the energy scale has been doubled for the deuterated sample, to illustrate the expected isotopic shift for D_2 molecules.

In order to further investigate the low-energy excitations, and in particular a mode occurring at 14.5 meV for the hydrogenous sample, higher-resolution measurements were carried out at both 100 and 300 K using the ILL IN6 spectrometer with an incident energy of 3.12 meV. Figure 7 shows the form of the vibrational densities of states at 100 K. The spectrum for the deuterated sample is repeated at the top with the energy transfer scale doubled (cf section 4.2). Further experiments on $Si_{0.78}H_{0.22}$ have been performed using the ISIS HET spectrometer at an incident energy of 50 meV. In this case the sample was cooled from room temperature as rapidly as possible (taking about 2 h) and then constant-temperature data were repeatedly recorded at regular intervals, mostly 2 h apart, observing the change in intensity of the para-H_2 and ortho-H_2 peaks (at 14.5 and 29.4 meV, respectively). These measurements were performed at stable temperatures of 19.3 and 35.6 K, for durations of 24 and 65 h, respectively. A period of 23 days was allowed between the two measurements to allow the distribution of H_2 molecules between the ortho and para states to resume its room-temperature state. The first and last spectra at 19.3 K are compared in figure 8.

A search has also been made for evidence of both translational and rotational hydrogen diffusion. This experiment was undertaken with a full width at half maximum (FWHM) energy resolution of 1.23 μeV, using the ILL IN10 instrument and an incident energy of 2.08 meV. The scattering in the region of the elastic line was recorded at 4 and 302 K, but no increase in width or change in peak shape was observed, as may be seen from figure 3(A) of [5], which compares the two elastic peak profiles after internormalization to the same maximum intensity. In addition, the profile at both temperatures is in excellent agreement with the

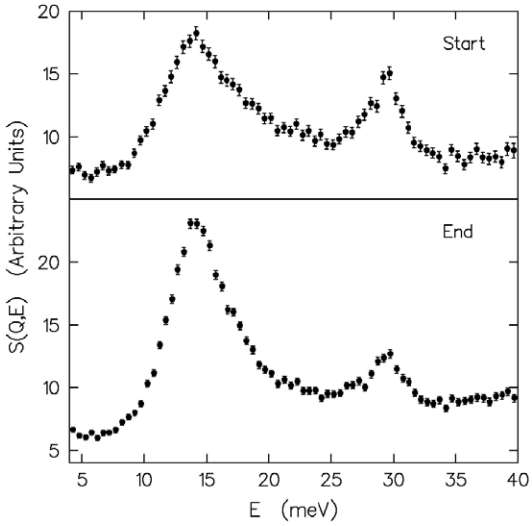

Figure 8. The time dependence of the peaks arising from the ortho (29.4 meV) and para (14.5 meV) rotational modes of H_2 molecules at 19.3 K. The upper spectrum was recorded for 30 min at a median time of 139 min, after cooling, and the lower curve was accumulated for 2 h at a median time of 1416 min.

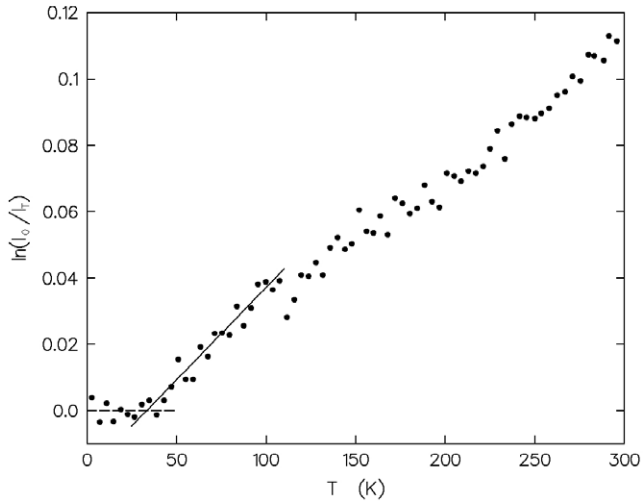

Figure 9. Quasi-elastic neutron scattering data for hydrogenated amorphous silicon from the IN10 spectrometer (ILL), showing the temperature dependence of the logarithm of the ratio of the elastic peak intensity at zero kelvin, I_0, to that at temperature T, I_T. ●: experimental data; dashed line: zero; and solid line: fit to the initial slope of $\ln(I_0/I_T)$.

instrumental resolution function as determined from a vanadium standard. A further experiment was performed to measure the temperature dependence of the Debye–Waller factor for the hydrogen atoms between 2 and 302 K by recording the scattering in a 1.23 μeV window at the elastic energy. The temperature dependence of the logarithm of the ratio of the intensity at zero kelvin to that at temperature T is shown in figure 9.

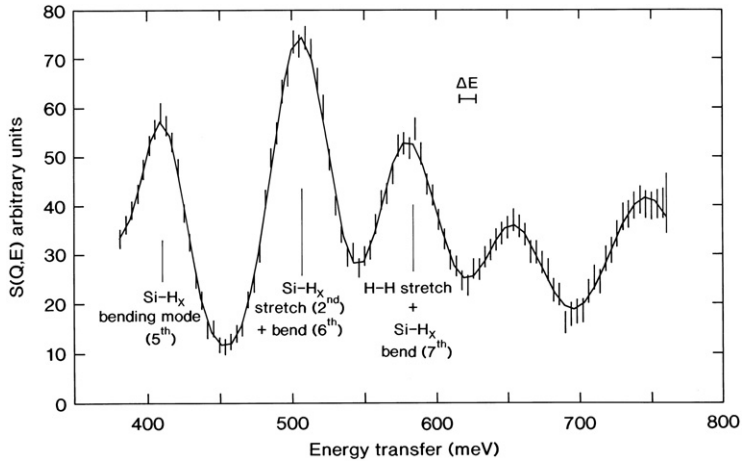

Figure 10. The high-energy transfer inelastic neutron scattering from hydrogenated amorphous silicon measured at 30 K with the MARI spectrometer (ISIS) and an incident neutron energy of 908 meV [5].

An experiment to look for the H–H stretch mode was performed using the ISIS MARI spectrometer with the sample at 22, 33 and 42 K and an incident energy of 908 meV [5]. These temperatures were chosen because of the solid-to-fluid phase transition mentioned in section 1. The observed spectra did not change over this temperature range, but this may just reflect the relatively low resolution of the neutron technique, in this energy range, compared to that of IR absorption spectroscopy. Summed data for the combined measurements are plotted in figure 10.

2.4. Small-angle neutron scattering

The SANS intensities were measured using the D17 instrument at the ILL. A helical slot velocity selector was employed to provide neutrons of wavelength, λ, equal to 9 and 12 Å, with a resolution $\Delta\lambda/\lambda$ of 10% (FWHM). The scattered intensity was recorded by a two-dimensional 128 × 128 cell multidetector (each cell 5 mm × 5 mm), which was positioned at distances of 0.85 and 2.5 m, respectively, for the two wavelengths, thus providing data in the scattering vector magnitude range $0.005 \leqslant Q \leqslant 0.4$ Å^{-1}. The powdered samples (2 mm thick) were contained in silica cells of rectangular cross section and wall thickness 0.5 mm. Background measurements were recorded for both an empty sample container and a cadmium absorber, which was used to determine the background component transmitted and therefore attenuated by the sample. Transmission cross sections were measured at each wavelength and a 1 mm thick water sample in a similar cell was employed to provide both the detector efficiency profile and a normalization standard, the latter by reference to the results of Hulme [70] for water normalized to a single-crystal vanadium plate. The full details of the data reduction are given in [7]. In addition to the normalization, it is also necessary to remove the incoherent-scattering contribution to the measured cross section for the hydrogenated sample. The uncertainty in the hydrogen content of this material (±2 at.%) introduces an additional error of the order of ±0.06 barns/str/atom into the corrected differential scattering cross section. As an example, the fully corrected SANS differential cross section for $Si_{0.77}D_{0.23}$, in the range $0.05 \leqslant Q \leqslant 0.4$ Å^{-1}, is shown in figure 11.

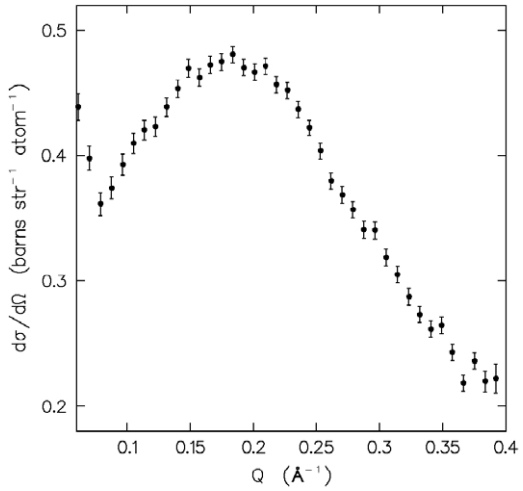

Figure 11. The fully corrected SANS for the $Si_{0.77}D_{0.23}$ sample in the region $0.05 \leqslant Q \leqslant 0.4$ Å^{-1}.

3. Diffraction

All three correlation functions in figure 4 exhibit peaks at 2.36 ± 0.02 and 3.84 ± 0.01 Å due to Si–Si bonds and the Si–(2)Si distance, respectively (cf table 1). In the case of $Si_{0.77}D_{0.23}$ and $Si_{0.78}H_{0.22}$, the features due to Si–H interactions can be easily identified since, for the hydrogenated sample, the peaks are negative, as a result of the negative value of $\bar{b}_H$. The first major peak occurs at 1.49 Å for $Si_{0.77}D_{0.23}$ and $Si_{0.78}H_{0.22}$ and arises from Si–D and Si–H bonds, respectively, while for $Si_{0.725}D_{0.120}F_{0.155}$ this peak is broader, and shifted to slightly higher r (1.55 Å), due to the presence of both Si–D and the longer Si–F bonds. Since the $Si_{0.77}D_{0.23}$ and $Si_{0.78}H_{0.22}$ samples are of the same composition, within the experimental uncertainty, and have been analysed with their average composition ($x = 0.225$), a simple subtraction of the data for $Si_{0.78}H_{0.22}$ from those for $Si_{0.77}D_{0.23}$ yields the D–H difference correlation function

$$\begin{aligned}\Delta T_{DH}(r) &= T_D(r) - T_H(r) \\ &= 2(1-x)\bar{b}_{Si}(\bar{b}_D - \bar{b}_H)t_{SiH}(r) + x(\bar{b}_D^2 - \bar{b}_H^2)t_{HH}(r)\end{aligned} \tag{1}$$

where

$$T_D(r) = (1-x)\bar{b}_{Si}^2 t_{SiSi}(r) + 2(1-x)\bar{b}_{Si}\bar{b}_D t_{SiH}(r) + x\bar{b}_D^2 t_{HH}(r) \tag{2}$$

and

$$T_H(r) = (1-x)\bar{b}_{Si}^2 t_{SiSi}(r) + 2(1-x)\bar{b}_{Si}\bar{b}_H t_{SiH}(r) + x\bar{b}_H^2 t_{HH}(r) \tag{3}$$

are, respectively, the total correlation functions for $Si_{0.77}D_{0.23}$ and $Si_{0.78}H_{0.22}$. $\Delta T_{DH}(r)$ is shown in figure 12, together with $T_D(r)$ and $T_H(r)$, and only involves Si–H and H–H correlations. Alternatively, it is possible to use a different weighting of the two data sets to obtain the Si–H + H–H difference correlation function

$$\Delta T_{Si}(r) = [\bar{b}_D T_H(r) - \bar{b}_H T_D(r)]/(\bar{b}_D - \bar{b}_H) = (1-x)\bar{b}_{Si}^2 t_{SiSi}(r) - x\bar{b}_D\bar{b}_H t_{HH}(r) \tag{4}$$

(figure 12, top), which is dominated by the Si–Si contribution and approximates the x-ray correlation function, $T^X(r)$.

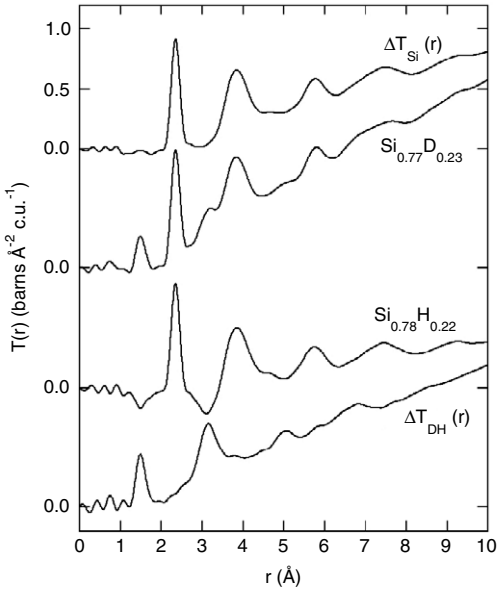

Figure 12. The real-space total correlation functions for $Si_{0.77}D_{0.23}$ and $Si_{0.78}H_{0.22}$ (Q_{max} = 28.485 Å^{-1}), together with the D–H difference correlation function, $\Delta T_{DH}(r)$, and the Si–Si + H–H difference, $\Delta T_{Si}(r)$.

Those features which increase in intensity in the D–H difference correlation function, $\Delta T(r)$, with respect to $T_D(r)$ are Si–H (or Si–D) correlations, and those which decrease in intensity are H–H (or D–D) correlations. Examination of this function aids a comparison with the previous lower-resolution ($Q_{max} = 16$ Å^{-1}) neutron diffraction measurements of Bellissent and co-workers [21–24]. In the latter investigation, all three component correlation functions (Si–Si, Si–H and H–H) were extracted by isotopic substitution, and a schematic diagram summarizing the distances identified in this work is reproduced in figure 13. There is good agreement between the Si–Si peaks at 2.36 and 3.84 Å, and a feature at 5.75 Å is also observed in both data sets. These peaks disappear in $\Delta T_{DH}(r)$ (figure 12) and so are conclusively Si–Si interactions. Analysis of $\Delta T_{DH}(r)$ shows the first two Si–H correlations at 1.48 and 3.2 Å. Both of these peaks are very sharp. The peak at 5.1 Å in $\Delta T_{DH}(r)$ was observed at 4.9 Å in the earlier study, where it appears as a much smaller, broader feature. A similar difference in position and broadness of the peak at 6.9 Å is also evident. As this region describes the intermediate-range order, small differences might be expected as a consequence of the different preparation techniques. In the earlier study, the H–H component correlation function was difficult to extract and is consequently very noisy. Despite this, the rather broad feature at 2.41 Å, assigned to the H–H separation in a $=SiH_2$ grouping, is also observed in $\Delta T_{DH}(r)$ as a shoulder on the leading edge of the second Si–H correlation. Assuming that the H–$\hat{\text{Si}}$–H angle is equal to the tetrahedral angle (109.47°), the Si–H bond length of 1.494 Å yields an H–H distance of 2.440 Å, whereas Bellissent *et al* [21–24] obtain a Si–H bond length of 1.48 Å and a H–H distance of 2.41 Å (figure 13).

The ESR data in table 2 for the hydrogenated and deuterated samples indicate very few broken bonds. Hence, assuming total coordination numbers of 4.0 and 1.0, respectively, for Si and H, the four component average coordination numbers are given by

$$n_{Si(Si)} = (4 - 5x + x_M)/(1 - x) \tag{5}$$

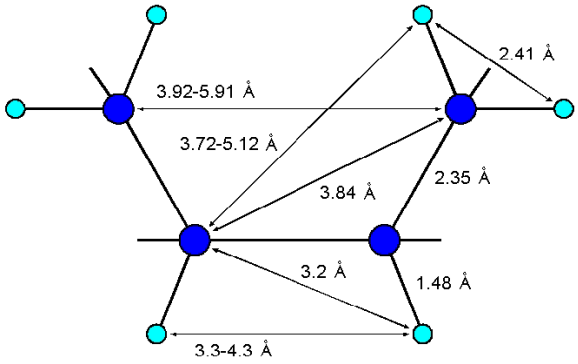

Figure 13. Interatomic distances in hydrogenated amorphous silicon, as identified by Bellissent and co-workers [21–24].

$$n_{\mathrm{Si(H)}} = (x - x_{\mathrm{M}})/(1 - x) \tag{6}$$

$$n_{\mathrm{H(Si)}} = (x - x_{\mathrm{M}})/x \tag{7}$$

and

$$n_{\mathrm{H(H)}} = x_{\mathrm{M}}/x \tag{8}$$

where x_{M} is the atomic fraction involved in H_2 molecules. The NMR data for the deuterated sample (table 2) give $x_{\mathrm{M}} = 0.03$. Thus, if x is taken to be the average value for the hydrogenated and deuterated samples ($x = 0.225$), the component coordination numbers become

$$n_{\mathrm{Si(Si)}} = 3.75 \tag{9}$$

$$n_{\mathrm{Si(H)}} = 0.25 \tag{10}$$

$$n_{\mathrm{H(Si)}} = 0.87 \tag{11}$$

and

$$n_{\mathrm{H(H)}} = 0.13. \tag{12}$$

The Si–D, Si–H, Si–F and Si–Si bond lengths, r_{ij}, were investigated by fitting the relevant peaks in $T(r)$ (figures 14 and 15), and the values obtained are summarized in table 3, together with the root mean square (rms) bond length variations, $(\overline{u_{ij}^2})^{1/2}$, and the coordination numbers, $n_{i(j)}$, where appropriate. As may be seen from the later figures 25 and 27 showing the component correlation functions for the structural models of Weaire *et al* [55, 56] and Winer and Wooten [58], there is a problem in fitting for the Si–Si bond length in that both Si–H and H–H interactions extend under the Si–Si peak. For this reason $n_{\mathrm{Si(Si)}}$ was initially fixed at the value given by equation (9), and a fit was performed to the low-r side of the peak. However, in the case of $Si_{0.77}D_{0.23}$ and $Si_{0.725}D_{0.120}F_{0.155}$, this led to a Si–Si bond length that was slightly shorter (2.337 ± 0.005 Å) than those obtained for $Si_{0.78}H_{0.22}$ and in previous studies of $Si_{1-x}H_x$ using x-rays and EXAFS spectroscopy (cf table 1). In addition, the fit residual had a well-defined peak at 2.48 Å. Since the models suggest that the Si–H and H–H contributions are relatively featureless, a second fit was performed to the full peak such that the residual was well behaved and yielded the parameters given in table 3. It should be noted, however, that the Si–H and H–H interactions contribute to the peak area and so it was not possible to extract $n_{\mathrm{Si(Si)}}$ from this latter fit. The Si–Si bond length and Si–(2)Si second-neighbour distance were also extracted

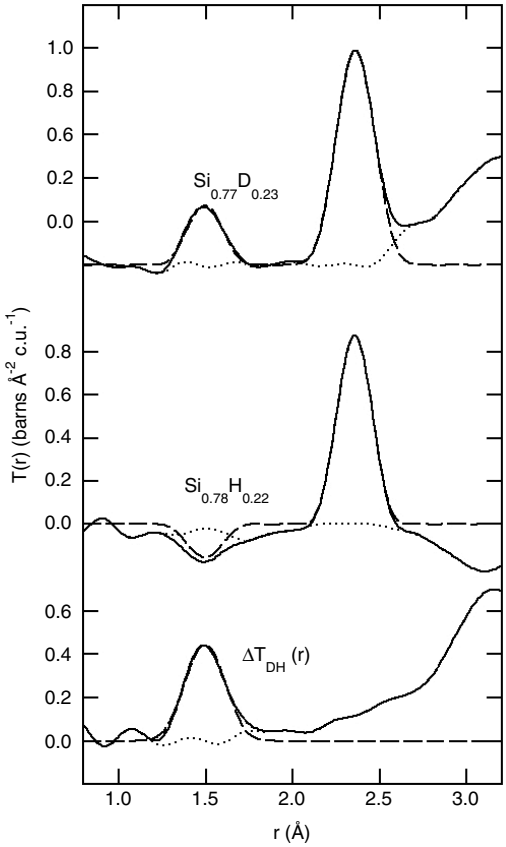

Figure 14. A fit to the Si–H (Si–D) and Si–Si peaks in $T_{\mathrm{D}}(r)$, $T_{\mathrm{H}}(r)$ and $\Delta T_{\mathrm{DH}}(r)$. ——: experimental data; - - - -: fit; and · · · · · ·: residual.

Table 3. Peak fits to the real-space correlation function, $T(r)$.

Sample	Bond	r_{ij} (Å)	$(\overline{u_{ij}^2})^{1/2}$ (Å)	$n_{i(j)}$
$Si_{0.77}D_{0.23}$	D–D	0.7414[a]	0.05[a]	1.00[a]
	Si–D	1.494 ± 0.005	0.066 ± 0.006	0.23 ± 0.01
	Si–Si	2.360 ± 0.002	0.082 ± 0.002	—
$Si_{0.78}H_{0.22}$	Si–H	1.494[a]	0.066[a]	0.23[a]
	Si–Si	2.355 ± 0.002	0.066 ± 0.002	—
$\Delta T_{\mathrm{DH}}(r)$	Si–H/D	1.495 ± 0.004	0.091 ± 0.004	0.28 ± 0.01
$\Delta T_{\mathrm{Si}}(r)$	Si–Si	2.357 ± 0.004	0.074 ± 0.005	—
	Si–(2)Si	3.854 ± 0.011	0.279 ± 0.008	—
$Si_{0.725}F_{0.155}D_{0.12}$	Si–D	1.497 ± 0.016	0.03 ± 0.05	0.17 ± 0.02
	Si–F	1.591 ± 0.013	0.060 ± 0.019	0.27 ± 0.03
	Si–Si	2.377 ± 0.004	0.085 ± 0.004	—

[a] Fixed.

from a fit to $\Delta T_{\mathrm{Si}}(r)$ (figure 16), but again it was not possible to extract $n_{\mathrm{Si(Si)}}$ due to the H–H contribution to $\Delta T_{\mathrm{Si}}(r)$.

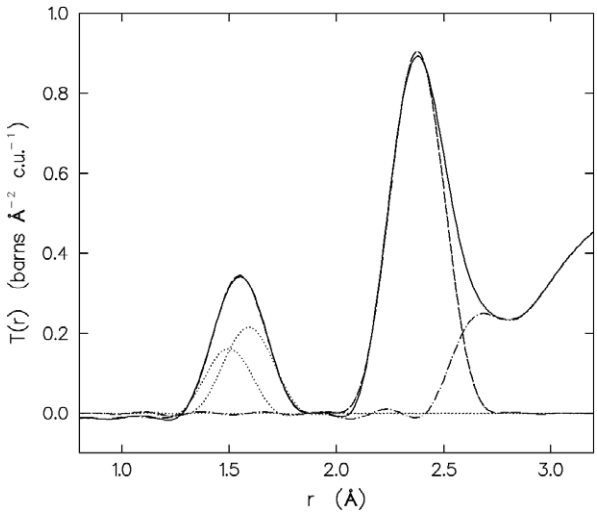

Figure 15. A fit to the first two peaks in the total correlation function for $Si_{0.725}D_{0.120}F_{0.155}$. ——: experimental data; - - - -: fit; · · · · · ·: individual peaks; and — · · —: residual.

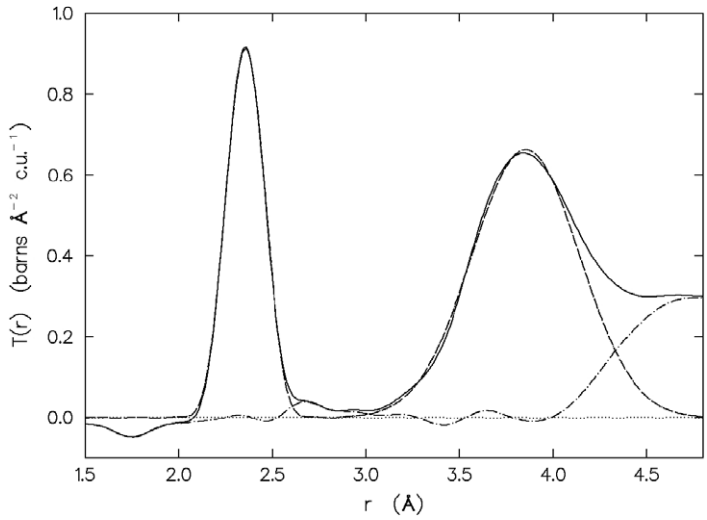

Figure 16. A fit to the first and second peaks in $\Delta T_{Si}(r)$. ——: experimental data; - - - -: fit; and — · —: residual.

A most interesting feature in $T_D(r)$ is the small peak at $r = 0.76$ Å, which is seen most clearly in figure 4 and is in the correct position to be attributed to the D–D bond length in the D_2 molecule. A careful examination of the other correlation functions shows that similar peaks are not apparent, but they may well be swamped by the higher noise levels. In the final D4b + LAD data, the peak still appears for $Si_{0.77}D_{0.23}$, and a peak now appears in the $Si_{0.78}H_{0.22}$ correlation function, although it only has the same intensity as the noise at lower r. This peak is slightly larger than the noise level at lower r, but is still quite prominent and symmetric. Its origin was therefore investigated by comparison with the expected peak if 3 at.% of the deuterium in $Si_{0.77}D_{0.23}$ is incorporated into D_2 molecules. The simulated peak uses the H–H bond length

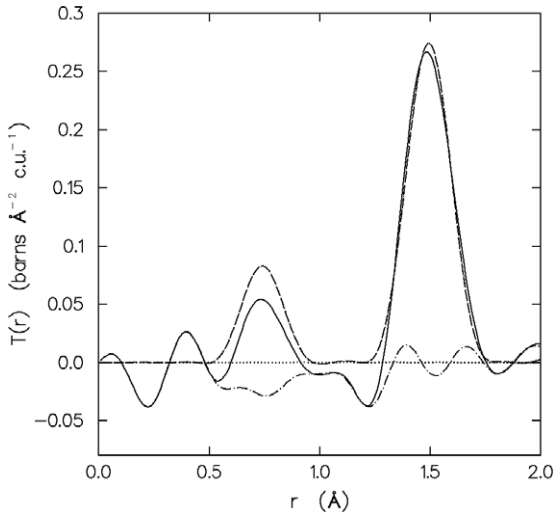

Figure 17. A fit to the first Si–D peak in $T_D(r)$, including the simulated intramolecular D–D peak at 0.74 Å, calculated assuming that 3 at.% of the deuterium in $Si_{0.77}D_{0.23}$ is incorporated into D_2 molecules. ——: experimental data; - - - -: fit; and — · —: residual.

from the literature (0.7414 Å [32]), together with an rms bond length variation of 0.05 Å, and is included with the fit to the Si–D bond length in figure 17. As may be seen, given the noise level, the simulated peak is in excellent agreement with the experimental data. The diffraction data could therefore be yielding a direct measurement of the D–D correlation in molecular D_2, but the noise levels are generally too high to be conclusive. The existence of D_2, DF or F_2 in amorphous $Si_{0.725}D_{0.120}F_{0.155}$ is not implied from the existence of D_2 in $Si_{0.77}D_{0.23}$ (or H_2 in $Si_{0.78}H_{0.22}$), because this material clearly does not follow the same deposition kinetics.

4. Inelastic neutron scattering

As indicated in section 2.3, a series of neutron inelastic and quasi-elastic scattering experiments has been performed to investigate specific energy transfer regions. Table 4 summarizes the energies of the various modes observed and compares these energies with the results of optical spectroscopy [61, 62]. These mode assignments are discussed in more detail in the following subsections.

4.1. Neutron-weighted vibrational density of states

For the deuterated sample, the ≡SiD and =SiD_2 stretching vibrations are partially resolved (figure 6) and so a two-peak fit was performed to the composite peak at ∼188 MeV, for both the HET and MARI data, and it is shown in figure 18. The resulting energies are given in table 5. The situation for the hydrogenated sample is more complicated in that the ≡SiH and =SiH_2 stretching modes are superimposed on a broad peak arising from the third harmonic of the Si–H bending vibration. Hence it was necessary to perform a three-peak fit, as illustrated in figure 19. For both samples, the fit is excellent, and it was unnecessary to include a contribution from –SiH_3 or –SiD_3 groups; i.e. there is no evidence for excitations corresponding to these groups in the neutron-weighted vibrational density of states.

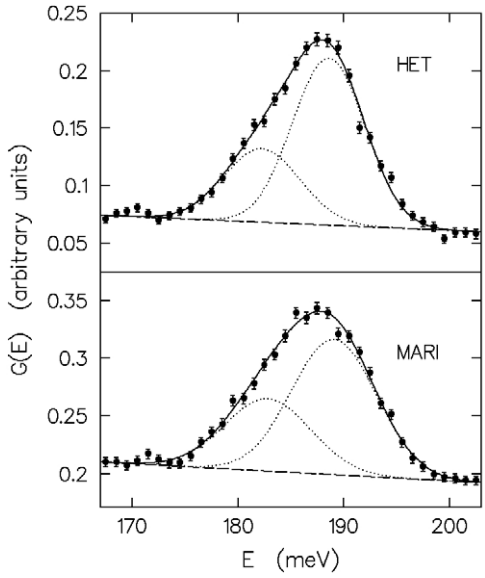

Figure 18. A fit to the ≡SiD and =SiD_2 stretch modes for the $Si_{0.77}D_{0.23}$ data in figure 6. ●: experimental data; ——: fit; · · · · · ·: individual peaks; and - - - -: background.

Table 4. Vibrational energies in amorphous $Si_{0.78}H_{0.22}$ and $Si_{0.77}D_{0.23}$ (in meV).

IR (Si–H)	Si–H (neutron)	Si–D (neutron)	Assignment[a]
		14.4	Si network
	14.5		Para-H_2 rotation
		19.1	Si network
27	29.4		Ortho-H_2 rotation
38	38	38	Si network
60	60	61	Si network
80	78	53	Si–H/D_n Rock & Wag
110	110	80	Si–H/D_2 bend
	159	111	Si–H/D_n 2nd Rock & Wag
		160	Si–D_2 2nd bend
248	251	183	Si–H/D stretch
260	259	189	Si–H/D_2 stretch
		240	Si–D_2 3rd bend
		295	—

[a] 2nd and 3rd refer to harmonics.

Table 5. Peak fit to Si–H/D stretch modes (in meV).

Sample	Instrument	Si–H/D	Si–H/D_2
$Si_{78}H_{22}$	HET	250.6	259.3
$Si_{77}D_{23}$	HET	182.3	188.6
$Si_{77}D_{23}$	MARI	182.8	189.1

It is interesting that the peaks for the ≡SiH and =SiH_2 stretching modes are significantly broader than the resolution of the instrument (FWHM = 3.3 meV) at this energy transfer—i.e. the stretch modes are not sharp and well defined. The present spectra can be analysed using

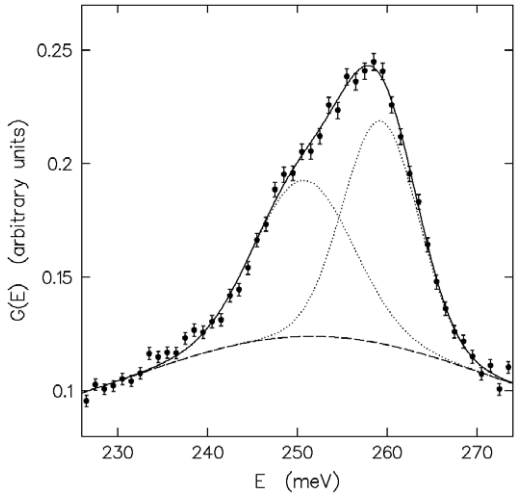

Figure 19. A fit to the ≡SiH and =SiH_2 stretch modes for the $Si_{0.77}H_{0.23}$ data in figure 6. Key as figure 16, except that the background includes a contribution from the third harmonic of the Si–H bending vibration.

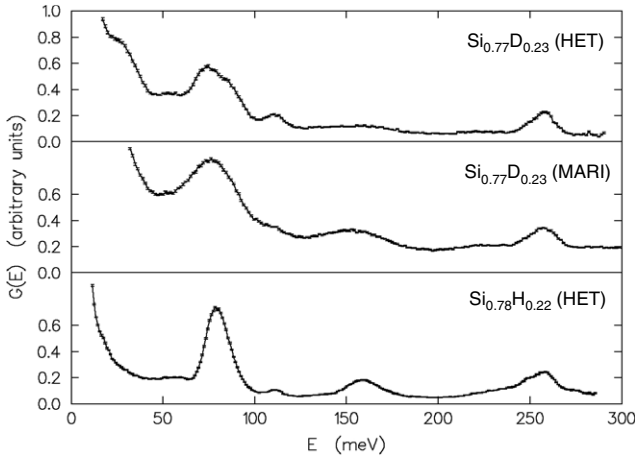

Figure 20. Inelastic neutron scattering data for $Si_{0.78}H_{0.22}$ and $Si_{0.77}D_{0.23}$ recorded with the HET and MARI spectrometers. The data are the same as those in figure 6, except that the energy scale for the $Si_{0.77}D_{0.23}$ sample is expanded by a factor of 1.373 (see the text).

theoretical neutron cross sections [71] and show that there are approximately equal numbers of ≡SiH and =SiH_2 groups. The average reduction in excitation energy introduced by deuteration is 1.373, which is slightly less than the factor of 1.414 ($\sqrt{2}$) expected for a hydrogen atom connected to an infinite mass, indicating the small but observable influence of the silicon matrix, as may be seen in figure 20, in which the energy scale for the $Si_{0.77}D_{0.23}$ sample is expanded by a factor 1.373. Because of the very large incoherent neutron cross section for hydrogen, the function for the hydrogenous sample is dominated by modes involving hydrogen motion while the distribution for the deuterated sample reflects both deuterium and silicon vibrations.

The =SiH_2 bending mode is observed at 110 meV, which is contrary to the results of Kamitakahara *et al* [72] who failed to observe this mode in a previous neutron experiment

and deduced that published conclusions from infra-red spectroscopy were wrong because of an abnormally large matrix element.

A large peak at 14.5 meV is observed for the hydrogenous sample [4], which had not been previously reported. Two earlier model calculations had predicted a peak at this energy: the first [48] involves a rotational mode of $-SiH_3$ groups and the second [49] a surface mode on large internal surfaces. Martinez and Yndurain [73] have also suggested that a mode at 214 cm^{-1} (26.5 meV) in the IR absorption spectrum of hydrogenated amorphous silicon is due to the presence of internal small ($\sim$7 atoms) surfaces associated with voids. However, as indicated above, there is no observable evidence in the full density of states for $-SiH_3$ groups in the present sample, and the surface mode suggestion is not compatible with the observed isotopic shift of a factor of $\sim$2 (cf below). As will be demonstrated in section 4.2, this peak does in fact arise from the rotation of H_2 molecules.

4.2. Low-energy excitations

Neither density of states obtained with the ILL IN6 spectrometer shows a pure Debye variation (E^2) as E tends to zero. As in the HET experiment, a strong peak is observed for the hydrogenated sample at 14.5 meV, while for the deuterated sample, the corresponding mode appears as a bulge on the side of the silicon density of states at about 7 meV (cf plot versus $2E$ at the top of figure 7). The Q dependence of the inelastic structure factor at this energy indicates that the mode is not associated with sound propagation and is of a localized nature, although experiments using a higher value of E_0 are strictly required to cover a larger range of Q, both for this mode and the rest of the low-energy transfer region so that unambiguous conclusions can be drawn. The isotopic shift of a factor of about two is consistent with an assignment as a rotation of molecular hydrogen.

The HET data for $Si_{0.78}H_{0.22}$, measured with an incident energy of 50 meV (figure 8), show peaks at 14.5 and 29.4 meV which arise from transitions between the rotational energy levels of H_2 molecules [74]. The first of these transitions (at 14.5 meV) is from the ground state with rotational quantum number $J = 0$, for which the molecules are in the para-hydrogen form (anti-parallel spins), to the $J = 1$ state, in which the molecules are in the ortho-hydrogen form (parallel spins). The second transition (at 29.4 meV) is from $J = 1$ (ortho-H_2) to $J = 2$ (para-H_2). The observation of these transitions is strong evidence that the sample contains molecular H_2. For a two-dimensional rotor, a peak would be observed at 7.3 meV, and its absence indicates that the H_2 molecules rotate in three dimensions, and are not constrained, as they would be if confined to a surface.

At room temperature the distribution of the H_2 molecules between the para-H_2 and ortho-H_2 states is given almost exactly by the degeneracies of the states, so the fraction of molecules in the ortho state, $c_o(0)$, is 0.749. However, when hydrogen is cooled there is a conversion to the para-H_2 ground state which, in the absence of a catalyst, occurs slowly over many hours. The intensities of the two INS peaks at 14.5 and 29.4 meV are proportional to the number of para-H_2 and ortho-H_2 molecules, and hence the evolution of these two peaks can be used to monitor the ortho–para conversion. The observation of this conversion in our data is further evidence of the presence of molecular hydrogen. Figure 21 shows the integral, $I_o(t)$, of the INS spectra from HET in the region of the ortho-H_2 peak at 29.4 meV, together with a fit of the following function [74]:

$$I_o(t) = B + \frac{Ac_o(0)}{Ktc_o(0) + 1}, \tag{13}$$

where K is the ortho–para conversion rate, A is a constant of proportionality, and B represents the background contribution to the spectrum in this region which arises from other processes.

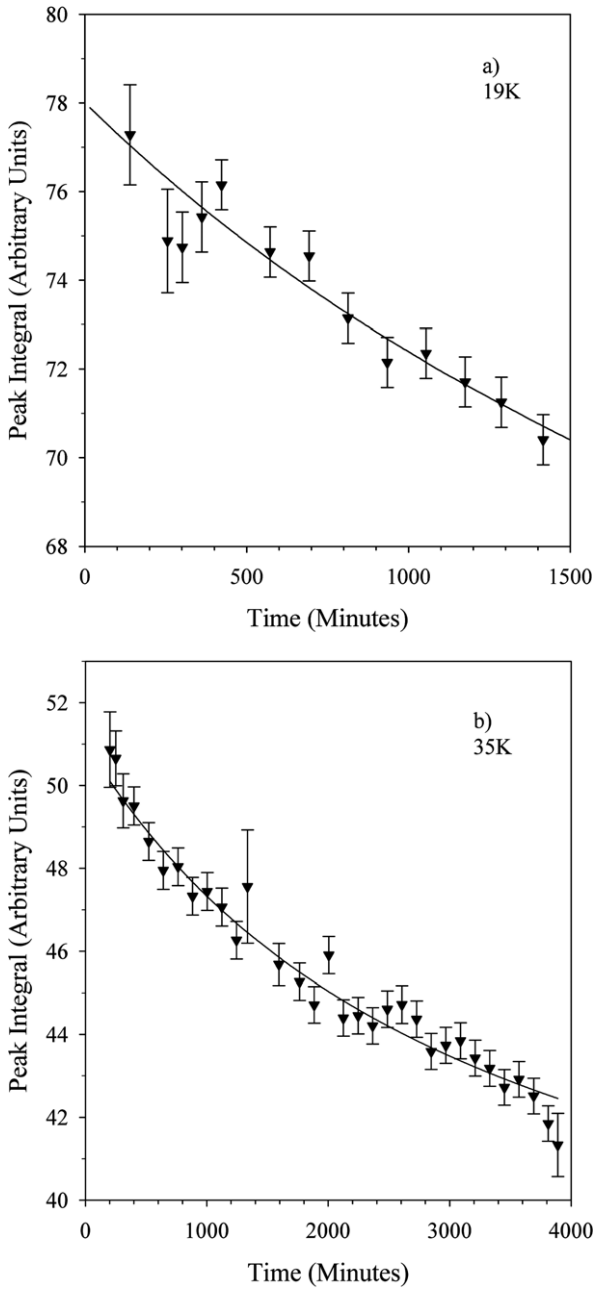

Figure 21. The time evolution of the integral from 25.5 to 32 meV of the INS spectra of $Si_{0.78}H_{0.22}$ measured on HET (points with error bars), together with the fit described in the text (smooth line), for data measured at temperatures of (a) 19.3, and (b) 35.6 K.

(The para-H_2 peak is not suitable for this analysis because it is too close to the elastic line for reliable results to be obtained.) The fits yielded values for the conversion rate, K, of $2.2 \pm 0.3\%$ and $2.4 \pm 0.2\%$ h^{-1} for temperatures of 19.3 and 35.6 K, respectively. The error for the 19.3 K

value is larger as a consequence of the shorter duration of the measurements. The quoted errors are based only on the errors on the peak integral, indicated by error bars in figure 21, and it is likely that the true errors are larger due to uncertainty in defining the time at which conversion starts. For an accurate determination of the conversion rate by this method, the data should be recorded for significantly longer than 1 day.

Our results show no significant change in the conversion rate for a temperature above and below the solid-to-fluid phase transition. Milenko *et al* [75] have used thermal conductivity to measure the ortho–para conversion rate for liquid and gaseous hydrogen over a wide range in temperature and pressure. Nevertheless, the values for the conversion rate, K, measured by Milenko *et al* at low temperature are not as high as those that we have determined, and a small extrapolation of their data is necessary for a comparison with our results. This extrapolation shows that our values for K are equivalent to a hydrogen density, ρ_{H}, of about 0.06 atom $\mathrm{\AA}^{-3}$.

4.3. Quasi-elastic neutron scattering

The quasi-elastic neutron scattering experiments show that the diffusion coefficients of all forms of hydrogen in amorphous $Si_{0.78}H_{0.22}$ remain very low up to 300 K. The temperature factor varies smoothly, giving no indication of the onset of hydrogen translational or rotational diffusion. The temperature dependence of the logarithm of the ratio of the intensity at zero kelvin to that at temperature T (figure 9) appears to start to increase significantly from its zero-kelvin value at ∼30 K. The fit to the initial slope above 30 K in figure 9 crosses the zero line at 33.5 K. This is extremely interesting in the light of the solid-to-fluid phase transition, which has been reported [49] at around 30 K for the molecular hydrogen occluded at high pressure in hydrogenated amorphous silicon.

4.4. High-energy excitations

The peak at 420 meV in figure 10 is the fifth overtone of the group of SiH_x bending modes around 80 meV, while the strong peak at 510 meV is the second overtone of the SiH_x stretch group at 250 meV. The peak at 570 meV can be assigned to the expected molecular hydrogen H–H stretch mode since its intensity is too large to be an overtone in the known sequences. As the resolution in E is 12 meV for this experiment, it is difficult to see how more detailed information can be gained by this technique for this mode without significantly improved instrumentation.

5. Small-angle neutron scattering

An increase below $Q \sim 0.04$ $\mathrm{\AA}^{-1}$ is observed in the scattered intensity from all three samples. A least-squares fit to a plot of $\ln(\mathrm{d}\sigma/\mathrm{d}\Omega)$ versus $\ln(Q)$ is consistent with a Q^4 dependence (cf figure 22), indicative of small-angle scattering in the Porod region [76]. The absence of an interference peak in this region means that the inhomogeneous regions can be treated as independent scatterers. Assuming that they have spherical symmetry or are randomly oriented, thus giving on average a spherical shape, a reverse Monte Carlo algorithm was employed to model the particle size distribution [7]. The results did not vary significantly between the three samples, and the final particle size distribution for amorphous $Si_{0.77}D_{0.23}$ is shown in figure 23. The particle radii exhibit a Lifshitz distribution of sizes [77], with most of the regions having a radius of ∼50 Å. The relative volume fractions of the variously sized particles calculated from this model indicates that, although regions in the size regime ∼50 Å are the most numerous, the

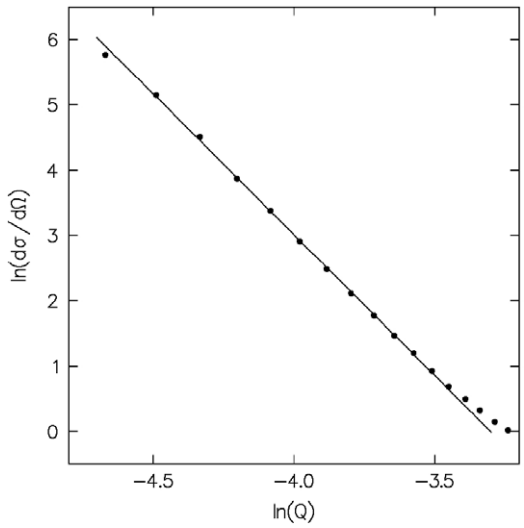

Figure 22. A $\ln(d\sigma/d\Omega)$ versus $\ln(Q)$ plot of the fully corrected SANS for the $Si_{0.77}D_{0.23}$ sample with $Q \leqslant 0.09$ Å^{-1}, together with a Porod fit (solid line). (The error bars are within the point symbols.)

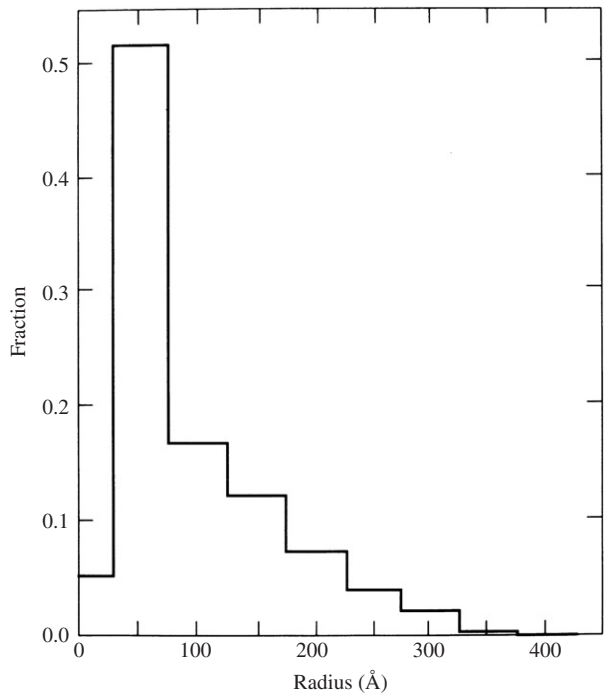

Figure 23. The particle size distribution obtained from a reverse Monte Carlo fit to the SANS data for $Si_{0.77}D_{0.23}$ [7].

majority of the volume fraction is made up of inhomogeneities in the range 150–300 Å. This size range is in good agreement with the results of Bellissent and co-workers [32–34, 36, 37].

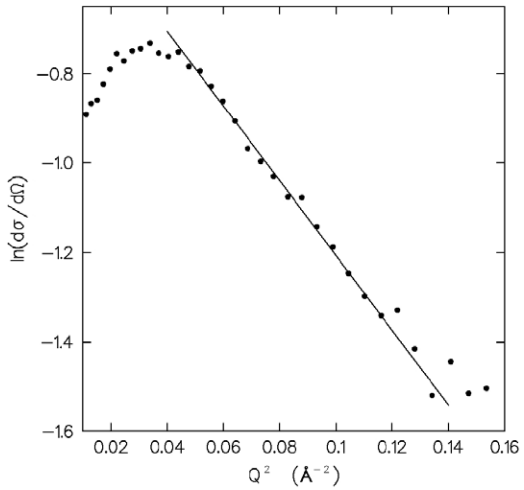

Figure 24. A Guinier plot of the SANS from $Si_{0.77}D_{0.23}$. ●: data; ——: fit.

Table 6. SANS parameters.

	$Si_{78}H_{22}$	$Si_{77}D_{23}$	$Si_{72.5}F_{15.5}D_{12}$
Guinier fit			
R_G (Å)	5.3 ± 0.2	4.9 ± 0.1	5.9 ± 0.1
C_G (barns/str/atom)	1.5 ± 0.1	0.66 ± 0.03	1.3 ± 0.1
R_S (Å)	6.8 ± 0.3	6.3 ± 0.2	7.6 ± 0.2
Inhomogeneities			
Q_P (Å^{-1})	0.166 ± 0.005	0.175 ± 0.005	0.227 ± 0.005
D_I (Å)	28.6 ± 0.8	27.5 ± 0.8	15.1 ± 0.8
ρ_I (10^{-5} Å^{-3})	1.02 ± 0.08	1.15 ± 0.08	6.91 ± 0.10
f_I (%)	1.37 ± 0.20	1.22 ± 0.02	12.8 ± 0.1

In addition to the SANS described above, the intensity from each sample displays an interference peak at higher Q (cf figure 11), which is much more pronounced than the 'weak diffraction ring' reported by Bellissent *et al* [32, 34, 35]. Figure 24 shows a Guinier plot of the data above the interference peak for the $Si_{0.77}D_{0.23}$ sample. A clearly defined Guinier region is visible. The position of the peak, Q_P, was obtained by the least-squares fitting of a third-order polynomial to the cross section data, and this position, the Guinier constant, C_G, and the radius of gyration, R_G, are summarized in table 6, together with the corresponding data for the $Si_{0.78}H_{0.22}$ and $Si_{0.725}D_{0.120}F_{0.155}$ samples. To allow the comparison with other studies, table 6 also includes the spherical radius, $R_S = (5/3)^{1/2} R_G$ [76].

The reciprocal-space peaks for $Si_{0.78}H_{0.22}$ and $Si_{0.77}D_{0.23}$ are at a slightly smaller value of Q than that (0.22 Å^{-1}) suggested by Bellissent *et al* [32, 34, 35], while the values of R_G for $Si_{0.78}H_{0.22}$ and $Si_{0.77}D_{0.23}$ correlate well with the SAXS values of Williamson *et al* [30] of ∼5 Å for inhomogeneities in non-device-quality material. The value of R_S calculated for the fluorinated sample does, however, seem to contradict the suggestion of Langford *et al* [54] that the radii of these regions increase from 5.2 to ∼15 Å on fluorination, the present data indicating a more modest rise from ∼6.6 to 7.6 Å.

Assuming a random distribution, the values of Q_P can be related to the average centre–centre separation of adjacent inhomogeneities, D_I, and hence the inhomogeneity number density, ρ_I, in the sample can be calculated [7, 76], together with the total (inhomogeneity) fraction, f_I, of the sample that is made up of these regions (see table 6). The calculated values of ρ_I for $Si_{0.78}H_{0.22}$ and $Si_{0.77}D_{0.23}$ are smaller than those found by Williamson *et al* [30] of $\sim 5 \times 10^{-5}$ Å^{-3}, but f_I for the fluorinated sample is in good agreement with that suggested by Langford *et al* [54] of 14–19%. The former discrepancy may be explained by differences in sample composition and/or preparation conditions.

From the definition of the Guinier constant, and making the approximation that the scattering length density of the matrix containing the inhomogeneities is equal to that of the bulk sample, $\langle c_S \rangle$, the scattering length density of the inhomogeneities, $\langle c_I \rangle$, may be obtained [7]. If it is assumed that the $Si_{0.78}H_{0.22}$ and $Si_{0.77}D_{0.23}$ samples are identical insofar as the internal structure of these inhomogeneities is concerned, the ratios of their scattering length densities can be directly related to the ratio of the average atomic scattering lengths in these regions. For these two component systems, the scattering length densities can be expanded in terms of the fractional composition, x_i, and neutron scattering length, $\bar{b}_i$, of each component atom. Moreover, since the samples are considered to be structurally identical, it follows that $x_H = x_D = x$, giving a value for x of either 0.0 ± 0.1 or 0.9 ± 0.1. This suggests that the regions in question are either precipitates of pure silicon or that they are largely hydrogen-filled cages.

To give the observed scattering, a silicon precipitate would need a density of 0.165 atom Å^{-3}, a value over three times higher than that of crystalline silicon, and hence these results show that the SANS arises from cages containing hydrogen only. A hydrogen density, again calculated from $\langle c_I \rangle$, gives $\rho_D = 0.10 \pm 0.01$ and $\rho_H = 0.13 \pm 0.02$ atom Å^{-3}, which is a factor two higher than the estimate from the kinetic studies described in section 4.2. These results are consistent with ∼140 hydrogen or deuterium atoms in each cage, a number much larger than would be expected purely from the hydrogen termination of broken Si bonds at the surface of the cage (<50 atoms). The surface of these cages can be expected [54] to be made up largely of Si atoms without broken bonds, suggesting that the large majority of the observed hydrogen must be in the form of molecular H_2. This assumption leads to a total H_2 content of ∼3 at.%, which is in excellent agreement with NMR measurements made on the $Si_{0.77}D_{0.23}$ sample (cf table 2). In addition, the value of ∼50–60 H_2 molecules per cage is consistent with that suggested by Chabal and Patel [49] of $\lesssim$100 molecules in any one cluster.

The density of hydrogen calculated for these materials is consistent with that for pressurized fluid hydrogen at 300 K and, assuming that the pressure–density phase relationship is the same as that for compressed fluid n-H_2 on the 300 K isotherm, it can be calculated that these densities correspond to a hydrogen pressure of ∼10 kbar in the deuterated material, and ∼25 kbar in the hydrogenated material [78]. The associated pressure increases exponentially with increasing density and, as a result, the ∼10% errors inherent in the density calculations give rise to a ∼70% uncertainty in the associated pressures. However, the values quoted above are not inconsistent with those from NMR data, which suggest a pressure of ∼2 kbar at cryogenic temperatures [48], and with the inelastic neutron scattering results outlined in section 4 [6].

It has been suggested [54] that the molecular SiF_4, known to exist in the fluorinated material [52], is contained as single isolated molecules in cages of much the same size as those observed here. If it is assumed that the scattering regions in the $Si_{0.725}D_{0.120}F_{0.155}$ sample are caused by a mixture of D_2-packed cages of the type found for $Si_{0.77}D_{0.23}$ and of the SiF_4-containing type suggested by Langford *et al* [54], the (measured) average scattering length

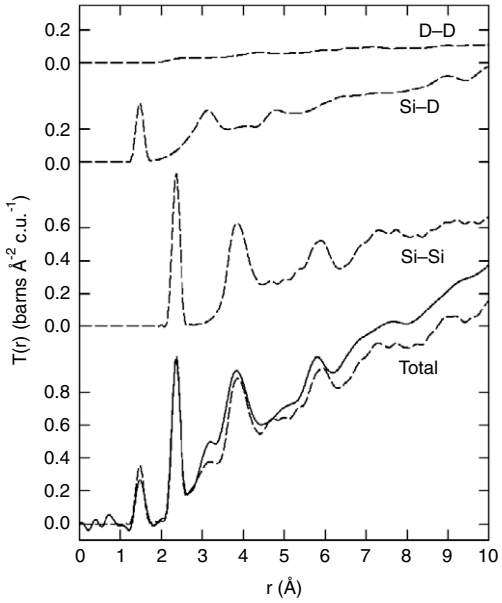

Figure 25. A comparison of the Weaire *et al* [55, 56] model (dashed lines) with the experimental total correlation function for the $Si_{0.77}D_{0.23}$ sample.

density for the inhomogeneities in this material is related to the scattering length densities of the two types of scattering centres and their fractional composition. The scattering length density of D_2-filled cages calculated above, the average scattering length for an SiF_4 molecule and the known cage volume then suggest that, if this particular model is correct, ∼98% of the cages contain an SiF_4 molecule. This percentage indicates that, within experimental uncertainties, the SANS observed from this material is consistent with a model of SiF_4-containing cages of largely the same size and distribution as those predicted by Langford *et al* [54]. Moreover, the similarity in the cage size observed for $Si_{0.77}D_{0.23}$ and $Si_{0.725}D_{0.120}F_{0.155}$, despite the vastly different internal pressures, suggests that inhomogeneities of these dimensions are inherent to the structure of the amorphous silicon matrix, rather than the result of the structures placed on it by the constituent gases.

6. Structural models

As indicated in section 1, random network models of hydrogenated amorphous silicon have been generated by Weaire *et al* [55, 56] and by Winer and Wooten [58]. The former is a cluster model and, to correct for the finite model size, it is necessary to limit the calculation of the component correlation functions, $t_{ij}(r)$, to the atoms contained within a sphere. In the case of the Weaire *et al* model, many of the H atoms are situated towards the edge, where the model density starts to decrease. Hence the choice of the diameter of the calculation sphere is a compromise between maintaining a sufficiently high density together with an adequate H content. The comparison with experiment was therefore performed with 390 atoms (314 Si and 76 H) included within a sphere of diameter 26.2 Å, yielding a composition $Si_{0.805}H_{0.195}$. This is slightly less H than the total in the present $Si_{0.78}H_{0.22}$ and $Si_{0.77}D_{0.23}$ samples, but is very close to the network composition, if it is assumed that 3 at.% of the H is present as H_2 molecules. Of the 76 H atoms, 8 are incorporated into (4) $=SiH_2$ groups. The component correlation functions

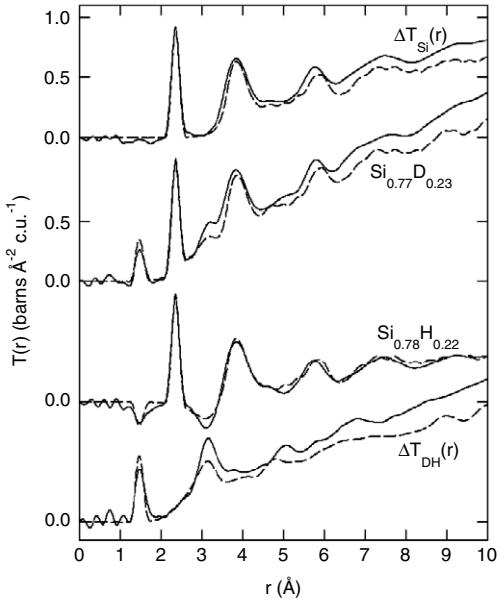

Figure 26. A comparison of the Weaire *et al* [55, 56] model (dashed lines) with the experimental total correlation function for $Si_{0.77}D_{0.23}$ and $Si_{0.78}H_{0.22}$, together with the D–H and Si–Si + H–H difference correlation functions (solid lines).

for the model were thermally broadened, weighted by the appropriate neutron scattering lengths and folded with the peak function, $P(r)$, which defines the experimental resolution in real space, before adding to give $T(r)$, as shown for the deuterated model in figure 25.

That the average number density for the chosen spherical cluster (0.041 42 c.u. $Å^{-3}$; $\rho^0_{Si} = 0.033\,34$ atoms $Å^{-3}$) is too low may be seen from the fact that the model $T(r)$ falls below the experimental data. Figure 26 compares the model with the total correlation functions for both the deuterated and hydrogenated samples, together with the D–H difference correlation function, $\Delta T_{DH}(r)$. The negative value of $\bar{b}_H$ leads to a fortunate cancellation of the effects of the incorrect density and composition, such that the average density contributions, $T^0(r)$, for the model and the hydrogenated sample almost coincide. Allowing for the density discrepancy, the main features in the correlation functions for the Weaire *et al* model are in good agreement with experiment, indicating that it is a very reasonable representation of the network component of the structure.

Since the Winer and Wooten [58] model has a periodic boundary, it is not necessary to correct for the finite model size, but the maximum value of r is limited to half of the minimum dimension of the unit cell ($r_{max} = 4.9$ Å). The average number density is 0.0575 c.u. $Å^{-3}$ ($\rho^0_{Si} = 0.0444$ atoms $Å^{-3}$) and the composition is $Si_{0.77}H_{0.23}$; i.e. identical to that of the present $Si_{0.77}D_{0.23}$ sample. The small number of atoms in the unit cell, combined with the imposition of periodic boundary conditions, means that the model network exhibits considerable strain/distortion, as may be seen from the experimental component correlation functions in figure 27 and the comparison with both samples and $\Delta T(r)$ in figure 28. For this reason, the Winer and Wooten model is not in as good agreement with experiment as that of Weaire *et al* [55, 56].

Winer and Wooten [58] have calculated the hydrogen atom vibrational density of states for their model (figure 4 of [58]). This exhibits a broad distribution of modes centred around

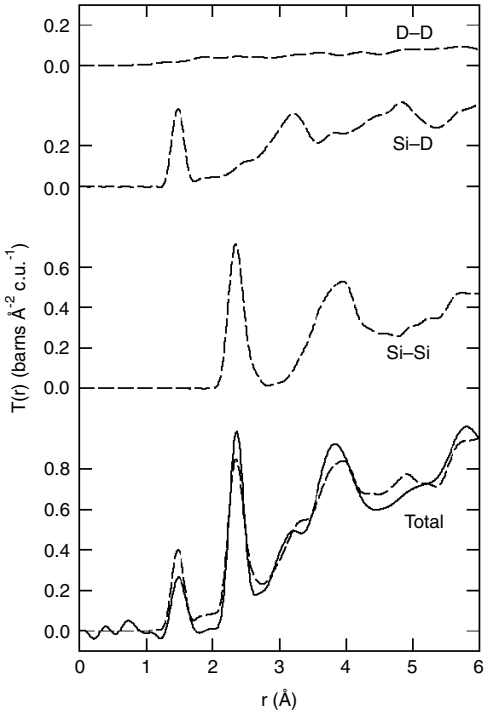

Figure 27. A comparison of the Winer and Wooten [58] model (dashed lines) with the experimental total correlation function for the $Si_{0.77}D_{0.23}$ sample.

85 meV, and extending from ∼45 to 125 meV, presumably including the Si–H rocking, wagging and bending vibrations (table 4). There is also a group of modes centred at 250 meV, corresponding to the Si–H stretching vibrations. Given the absence of H_2 molecules in the model, a small peak at 22 meV, which is much more intense in the full vibrational density of states, presumably arises from vibrations of the silicon network.

7. Conclusions

The present suite of neutron scattering experiments confirms the results of previous studies which suggest a close relationship between the network structure of hydrogenated amorphous silicon and that of evaporated amorphous silicon. In the hydrogenous material, the broken bonds of the latter are saturated with H atoms to form approximately equal numbers of ≡SiH and =SiH_2 groups. The number of –SiH_3 groups in the present samples is small (<1 at.% H), and they were not detected in the inelastic neutron scattering experiments. The network of $Si_{0.78}H_{0.22}$ and $Si_{0.77}D_{0.23}$ is well represented by the structural model of Weaire *et al* [55, 56].

The inelastic neutron scattering experiments unambiguously demonstrate the existence of high-pressure molecular H_2 (D_2) trapped in the cages of the amorphous network at high densities and at pressures of the order of ∼10–20 kbar at ambient temperature, as shown by the observation of the ortho–para conversion at low T, via the molecular rotation modes at 14.5 and 29.4 meV. Further neutron scattering evidence for the existence of H_2 (D_2) molecules in the present samples is afforded by the neutron diffraction data for the deuterated sample, which exhibit a small feature at the expected intramolecular D–D distance, and the SANS

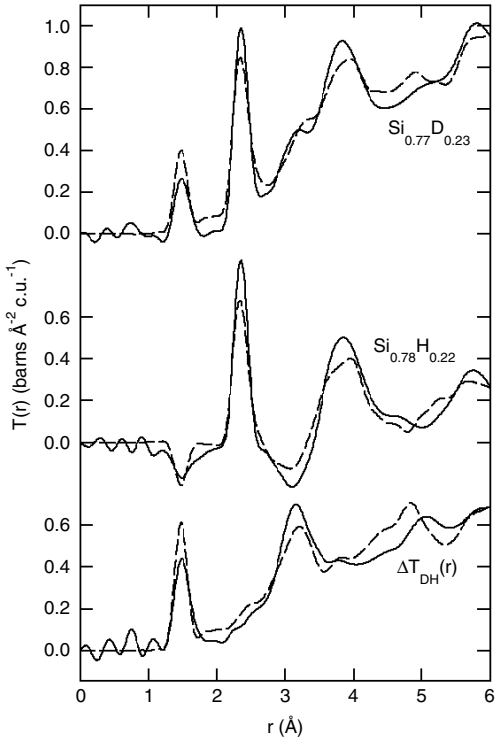

Figure 28. A comparison of the Winer and Wooten [58] model (dashed lines) with the experimental total correlation function for $Si_{0.77}D_{0.23}$ and $Si_{0.78}H_{0.22}$, together with the D–H difference correlation function (solid lines).

experiments, which indicate the presence of H_2 (D_2) filled cages, with each cage containing, on average, ∼50–60 H_2 molecules. In addition, further inhomogeneities are observed with effective spherical radii up to 450 Å and a Lifshitz distribution of sizes.

The use of silicon tetrafluoride in the feedstock during the deposition process, on the other hand, produces a material whose network short-range order is unlikely to differ greatly from that of hydrogenated amorphous silicon, suggesting that the previously observed differences in electronic behaviour between these materials may be due in some part to this change in cage content. The SANS data for the $Si_{0.725}D_{0.120}F_{0.155}$ sample are consistent with a cage structure containing mainly isolated SiF_4 molecules.

Acknowledgments

This work was supported by the Engineering and Physical Sciences Research Council (UK) using facilities at the Institut Laue-Langevin and the Rutherford Appleton Laboratory. The authors would also like to thank D Weaire and F Wooten for supplying the coordinates of their models.

References

[1] Street R A 1991 *Hydrogenated Amorphous Silicon* (Cambridge: Cambridge University Press)
[2] Street R A 1993 *Phys. World* **6** (4) 54
[3] Howells W S 1986 *Ann. Chim. Fr. Sci. Mater.* **11** 691

[4] Sinclair R N, Wright A C, Brunier T M, Hulme R A, Guy C A, Hannon A C and Arai M 1992 *J. Non-Cryst. Solids* **150** 219
[5] Wright A C, Brunier T M, Guy C A, Sinclair R N, Hannon A C and Jansen F 1993 *Physica* A **201** 395
[6] Sinclair R N, Wright A C, Brunier T M, Hannon A C, Bennington S M and Jansen F 1995 *J. Non-Cryst. Solids* **192/193** 243
[7] Guy C A, Wright A C, Sinclair R N, Stewart R J and Jansen F 1996 *J. Non-Cryst. Solids* **196** 260
[8] Knights J C 1984 Structural and chemical characterization *The Physics of Hydrogenated Amorphous Silicon I Structure, Preparation and Devices* (*Springer Topics in Applied Physics* vol 55) ed J D Joannopoulos and G Lucovsky (Berlin: Springer) pp 5–62
[9] Elliott S R 1989 *Adv. Phys.* **38** 1
[10] Polk D E and Boudreaux D S 1973 *Phys. Rev. Lett.* **31** 92
[11] Wooten F and Weaire D 1987 *Solid State Phys.* **40** 1
[12] Etherington G, Wright A C, Wenzel J T, Dore J C, Clarke J H and Sinclair R N 1982 *J. Non-Cryst. Solids* **48** 265
[13] Wright A C, Hulme R A, Grimley D I, Sinclair R N, Martin S W, Price D L and Galeener F L 1991 *J. Non-Cryst. Solids* **129** 213
[14] Solomon I 1979 Spin effects in amorphous semiconductors *Amorphous Semiconductors* (*Springer Topics in Applied Physics* vol 36) ed M H Brodsky (Berlin: Springer) pp 189–213
[15] Taylor P C 1984 Magnetic resonance measurements in a-Si:H *Hydrogenated Amorphous Silicon, Part C, Electronic and Transport Properties* (*Semiconductors and Semimetals* vol 21) ed J I Pankove (Orlando, FL: Academic) pp 99–154
[16] Mosseri R, Sella C and Dixmier J 1979 *Phys. Status Solidi* a **52** 475
[17] Schülke W 1981 *Phil. Mag.* B **43** 451
[18] Barna Á, Barna P B, Radnóczi G, Tóth L and Thomas P 1977 *Phys. Status Solidi* a **41** 81
[19] Graczyk J F 1979 *Phys. Status Solidi* a **55** 231
[20] Postol T A, Falco C M, Kampwirth R T, Schuller I K and Yelon W B 1980 *Phys. Rev. Lett.* **45** 648
[21] Bellissent R, Chenevas-Paule A, Chieux P and Menelle A 1985 *J. Non-Cryst. Solids* **77/78** 213
[22] Bellissent R 1986 *Ann. Chim. Fr. Sci. Mater.* **11** 699
[23] Menelle A 1987 *PhD Thesis* University of Paris VI
[24] Bellissent R, Menelle A, Howells W S, Wright A C, Brunier T M, Sinclair R N and Jansen F 1989 *Physica* B **156/157** 217
[25] Filipponi A, Della Sala D, Evangelisti F, Balerna A and Mobilio S 1986 *J. Physique Coll.* **47** C8 375
[26] Bellissent R, Chenevas-Paule A, Lagarde P, Bazin D and Raoux D 1983 *J. Non-Cryst. Solids* **59/60** 237
[27] Menelle A, Flank A M, Lagarde P and Bellissent R 1986 *J. Physique Coll.* **47** C8 379
[28] D'Antonio P and Konnert J H 1979 *Phys. Rev. Lett.* **43** 1161
[29] Leadbetter A J, Rashid A A M, Richardson R M, Wright A F and Knights J C 1980 *Solid State Commun.* **33** 973
[30] Williamson D L, Mahan A H, Nelson B P and Crandall R S 1989 *J. Non-Cryst. Solids* **114** 226
[31] Leadbetter A J, Rashid A A M, Colenutt N, Wright A F and Knights J C 1981 *Solid State Commun.* **38** 957
[32] Bellissent R, Chenevas-Paule A and Roth M 1983 A small-angle neutron scattering study of structural heterogeneities in a-Si:H *The Structure of Non-Crystalline Materials 1982* ed P H Gaskell, J M Parker and E A Davis (London: Taylor and Francis) pp 582–8
[33] Bellissent R, Chenevas-Paule A and Roth M 1983 *J. Non-Cryst. Solids* **59/60** 229
[34] Bellissent R, Chenevas-Paule A and Roth M 1983 *Physica* B **117/118** 941
[35] Chenevas-Paule A 1984 Experimental determination of structure *Hydrogenated Amorphous Silicon, Part A, Preparation and Structure* (*Semiconductors and Semimetals* vol 21) ed J I Pankove (Orlando, FL: Academic) pp 247–71
[36] Bellissent R 1987 *J. Non-Cryst. Solids* **97/98** 329
[37] Menelle A 1987 *J. Non-Cryst. Solids* **97/98** 337
[38] Knights J C and Lujan R A 1979 *Appl. Phys. Lett.* **35** 244
[39] Leopold D J, Boyce J B, Fedders P A and Norberg R E 1982 *Phys. Rev.* B **26** 6053
[40] Leopold D J, Coughlan B S, Fedders P A, Norberg R E, Boyce J B and Knights J C 1984 *J. Non-Cryst. Solids* **66** 121
[41] Boyce J B and Stutzman M 1985 *Phys. Rev. Lett.* **54** 562
[42] Boyce J B, Stutzmann M and Ready S E 1985 *J. Non-Cryst. Solids* **77/78** 265
[43] Bork V P, Fedders P A, Norburg R E, Boyce J B and Stutzmann M 1985 *J. Non-Cryst. Solids* **77/78** 711
[44] Leopold D J, Fedders P A, Norberg R E, Boyce J B and Knights J C 1985 *Phys. Rev.* B **31** 5642
[45] Boyce J B, Ready S E, Stutzmann M and Norberg R E 1989 *J. Non-Cryst. Solids* **114** 211
[46] Santos-Filho P, Volz M P, Corey R L, Kim Y W, Fedders P A, Norberg R E, Turner W and Paul W 1989 *J. Non-Cryst. Solids* **114** 235

[47] Su T, Chen S, Taylor P C, Crandall R S and Mahan A H 2000 *Phys. Rev.* B **62** 12849
[48] Chabal Y J and Patel C K N 1984 *Phys. Rev. Lett.* **53** 210
[49] Chabal Y J and Patel C K N 1984 *Phys. Rev. Lett.* **53** 1771
[50] Lide D R (ed) 2006 *CRC Handbook of Chemistry and Physics* 87th edn (Boca Raton, FL: Taylor and Francis)
[51] Matsumura H, Sakai K, Kawakyu Y and Furukawa S 1981 *J. Appl. Phys.* **52** 5537
[52] Janai M, Weil R and Pratt B 1983 *J. Non-Cryst. Solids* **59/60** 743
[53] Shimizu T, Kumeda M, Komatsu H and Yonezawa Y 1985 *J. Non-Cryst. Solids* **77/78** 719
[54] Langford A A, Mahan A H, Fleet M L and Bender J 1990 *Phys. Rev.* B **41** 8359
[55] Weaire D, Higgins N, Moore P and Marshall I 1979 *Phil. Mag.* B **40** 243
[56] Weaire D and Wooten F 1980 *J. Non-Cryst. Solids* **35/36** 495
[57] Guttman L 1981 *Phys. Rev.* B **23** 1866
[58] Winer K and Wooten F 1983 *J. Non-Cryst. Solids* **59/60** 193
[59] Sadoc J F and Mosseri R 1982 *Phil. Mag.* B **45** 467
[60] Rivier N and Duffy D M 1982 *J. Physique* **43** 293
[61] Lucovsky G and Pollard W B 1984 Vibrational properties of amorphous alloys *The Physics of Hydrogenated Amorphous Silicon II Electronic and Vibrational Properties* (*Springer Topics in Applied Physics* vol 56) ed J D Joannopoulos and G Lucovsky (Berlin: Springer) pp 301–55
[62] Zanzucchi P J 1984 The vibrational spectra of a-Si:H *Hydrogenated Amorphous Silicon, Part B, Optical Properties* (*Semiconductors and Semimetals* vol 21) ed J I Pankove (Orlando: Academic) pp 113–40
[63] Arai M, Taylor A D, Bennington S M and Bowden Z 1992 MARI—a new spectrometer for liquid and amorphous materials *Recent Developments in the Physics of Fluids* ed W S Howells and A K Soper (Bristol: Adam Hilger) pp F321–8
[64] Chen I and Jansen F 1983 *J. Non-Cryst. Solids* **59/60** 695
[65] Ley L 1984 Photoemission and optical properties *The Physics of Hydrogenated Amorphous Silicon II Electronic and Vibrational Properties* (*Springer Topics in Applied Physics* vol 56) ed J D Joannopoulos and G Lucovsky (Berlin: Springer) pp 61–168
[66] Straumanis M E and Aka E Z 1952 *J. Appl. Phys.* **23** 330
[67] Sears V F 1992 *Neutron News* **3** 26
[68] Wright A C 1993 Neutron and x-ray amorphography *Experimental Techniques of Glass Science* ed C J Simmons and O H El Bayoumi (Westerville: American Ceramic Society) chapter 8, pp 205–314
[69] Johnson P A V, Wright A C and Sinclair R N 1983 *J. Non-Cryst. Solids* **58** 109
[70] Hulme R A 1991 *PhD Thesis* Reading University
[71] Barrio R, Elliott R J and Thorpe M F 1983 *J. Phys. C: Solid State Phys.* **16** 3425
[72] Kamitakahara W A, Shanks H R, McClelland J F, Buchenau U, Gompf F and Pintschovius L 1984 *Phys. Rev. Lett.* **52** 644
[73] Martinez E and Yndurain F 1983 *Physica* B **117/118** 935
[74] Silvera I F 1980 *Rev. Mod. Phys.* **52** 393
[75] Milenko Y Y, Sibileva R M and Strzhemechny M A 1997 *J. Low Temp. Phys.* **107** 77
[76] Stewart R J 1986 Neutron scattering from defects in materials *Defects in Solids—Modern Techniques* ed A V Chadwick and M Terenzi (New York: Plenum) pp 95–130
[77] Lifshitz I M and Slyozov V V 1961 *J. Phys. Chem. Solids* **19** 35
[78] Shimizu H, Brody E M, Mao H K and Bell P M 1981 *Phys. Rev. Lett.* **47** 128